

The TESS Input Catalog and Candidate Target List [ver. 20170531]

Keivan G. Stassun^{1,2,3}, Ryan J. Oelkers^{1,2}, Joshua Pepper^{4,2}, Martin Paegert^{5,2}, Nathan De Lee^{6,2}, Guillermo Torres⁵, David Latham⁵, Philip Muirhead⁷, Courtney Dressing⁸, Barbara Rojas-Ayala⁹, Andrew Mann¹⁰, Scott Fleming¹¹, Al Levine¹², Roberto Silvotti¹³, Peter Plavchan¹⁴,
and the TESS Target Selection Working Group

ABSTRACT

The Transiting Exoplanet Survey Satellite (TESS) will be conducting a nearly all-sky photometric survey over two years, with a core mission goal to discover small transiting exoplanets orbiting nearby bright stars. It will obtain 30-minute cadence observations of all objects in the TESS fields of view, along with 2-minute cadence observations of 200,000 to 400,000 selected stars. The choice of which stars to observe at the 2-min cadence is driven by the need to detect small transiting planets, which leads to the selection of primarily bright, cool dwarfs. We describe the catalogs assembled and the algorithms used to populate the TESS Input Catalog (TIC). We also describe a ranking system for all stars in the sky according to the smallest transiting planet detectable, and assemble a Candidate Target List (CTL) using that ranking. We discuss additional factors that affect the ability to photometrically detect and dynamically confirm small planets, and we note additional stellar populations of special interest that may be added to the final target list. The TIC is available on the STScI MAST server, and an enhanced CTL is available through the Filtergraph data visualization portal system at filtergraph.vanderbilt.edu/tess_ctl.

1. Introduction

Essential to the success of the TESS mission is the creation of a TESS Input Catalog (TIC), a catalog of luminous sources on the sky. The purpose of the TIC is to enable the selection of optimal targets for the planet transit search, to enable calculation of flux contamination in the TESS aperture for each target, and to provide the most accurate stellar and planetary radii estimates, which will determine which targets receive mission-funded photometric and spectroscopic follow-up. The TIC is also essential for the community

¹Vanderbilt University

²Vanderbilt Initiative in Data-intensive Astrophysics (VIDA)

³Fisk University

⁴Lehigh University

⁵Harvard-Smithsonian Center for Astrophysics

⁶Northern Kentucky University

⁷Boston University

⁸Caltech

⁹Universidad Andrés Bello

¹⁰University of Texas

¹¹Space Telescope Science Institute

¹²Massachusetts Institute of Technology

¹³Osservatorio Astrofisico di Torino

¹⁴George Mason University

to select potential additional targets through the Guest Investigator program. We have created the TIC to contain every optically luminous, persistent object in the sky down to the limits of the available wide-field photometric catalogs (point source and extended source). We have therefore not included objects without significant persistent optical flux. We have also not included, for technical and logistical reasons, objects that move rapidly enough that their celestial positions cannot be calculated with linear proper motions. Therefore, we do not include solar system objects such as planets, asteroids, TNOs, etc.

The purpose of the TIC incorporates four basic needs. They are:

1. Similar to what the *Kepler* Input Catalog (KIC; Brown et al. 2011), the Ecliptic Plane Input Catalog (EPIC; Huber et al. 2016), and the NASA Exoplanet Archive (NEA) together provide for *Kepler* and *K2*, the TIC should include basic astronomical information for all sources in the TESS footprint, which means the entire sky. It is a catalog in which anyone can look up information about any object for which the TESS mission produces a light curve.
2. Enable selection of primary transit-search (i.e., 2-min cadence) targets for TESS. The incorporation of all luminous objects in the sky for the full TIC will allow a calculation of the flux contamination for all potential TESS targets. In practice, that involves a flux contamination value for every element in the Candidate Target List (CTL; see Sec. 3) subset of the TIC.
3. Provide stellar parameter information for the TESS Science Processing Operations Center (SPOC) to evaluate exoplanet transit candidates. As TESS gathers data and the light curves are searched for transit candidates, information about the target star, such as the effective temperature (T_{eff}), the surface gravity ($\log g$), the mass (M_{\star}), the radius (R_{\star}), and other parameters are used to calculate the planet properties.
4. Enable false positive determination. Both the SPOC and the public will need to be able to query the TIC to obtain a list of all known sources within some radius of any object in the TIC, with their accompanying information. That will allow users to decide how likely it is that signals in the light curve of a target are due to an astrophysical source that is not the target.

From the TIC we construct a prioritized CTL, from which the final 2-min cadence target stars are selected. Priorities are established via a scheme that emphasizes detectability of small planets. In the following sections, we detail the construction of the TIC (Section 2) and of the CTL (Section 3). For both the TIC and the CTL we describe the algorithms used to determine associated stellar parameters. We also describe the target prioritization scheme for the CTL. We conclude in Section 4 with a discussion of known limitations in the current TIC and CTL, as well as planned future improvements. The TIC and CTL are also accompanied by official release notes, which are provided in Appendix A. Public access to the TIC is provided via the MAST server, and access to an enhanced CTL is provided via the Filtergraph data visualization service at filtergraph.vanderbilt.edu/tess-ctl.

2. The TESS Input Catalog (TIC)

The TIC includes a number of columns, each with a specified format and a permitted range of values. These are summarized in Appendix B. The provenance flags associated with various TIC quantities are listed in Appendix C. Steps taken to ensure internal consistency among various TIC quantities are given in Appendix D. In this section we detail the procedures by which we have constructed the TIC, with particular detail provided regarding the algorithms, relations, and rules adopted for populating the TIC.

2.1. Assembly of the TIC

The process by which the various photometric catalogs have been assembled for the construction of the overall TIC (currently version 5) is summarized graphically in Figure 1. The compilation of the TIC is the product of merging three base catalogs to create a full list of point sources, extended sources, and other special objects that could be observed by TESS. We provide the quality flags from the base catalogs in the TIC but do not include the quality flags from the other assorted catalogs. This means the TIC inherits structure and biases from these catalogs as we describe in Section 4.2.

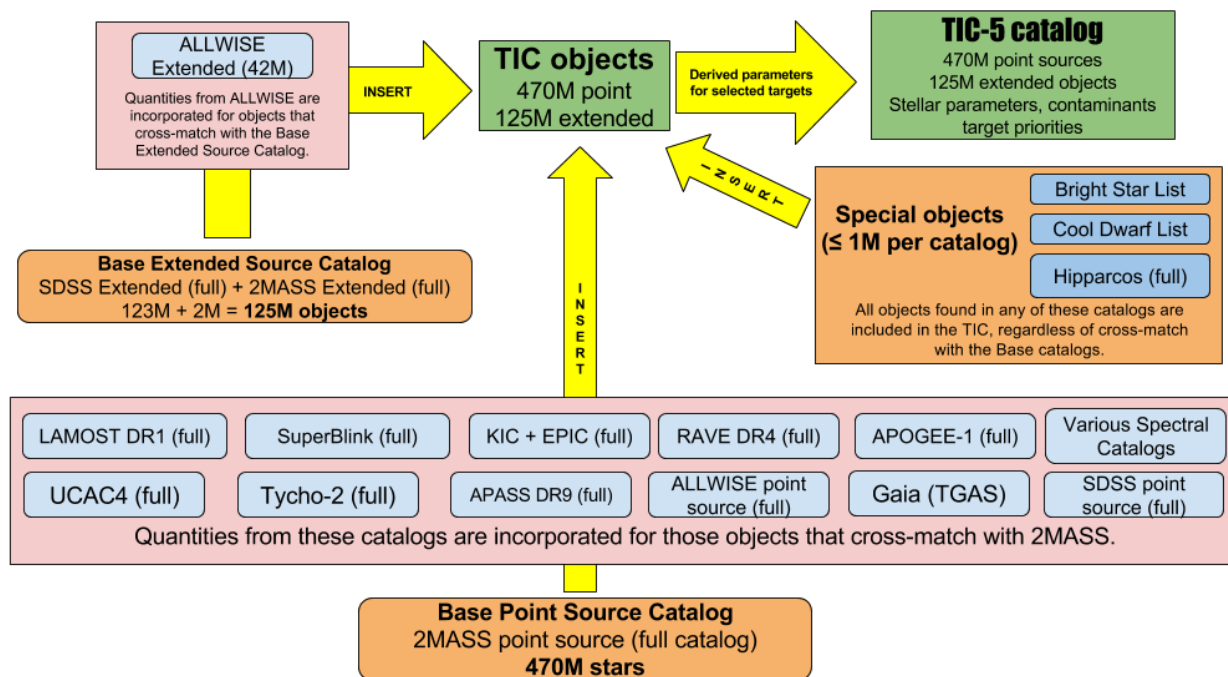


Fig. 1.— Visual overview of the photometric catalogs used to construct the overall TESS Input Catalog (TIC). Yellow arrows depict the order in which catalogs are cross-matched and/or merged. The final TIC (current version indicated by the integer number) is represented by the green box at the upper right.

In the first step the point source base catalog is constructed from the full 2MASS point source catalog (Skrutskie et al. 2006) of $\sim 470 \times 10^6$ objects. Next, this catalog is cross-matched against the following catalogs: LAMOST-DR1 (Luo et al. 2015), KIC+EPIC (Brown et al. 2011; Huber et al. 2016), RAVE (Boeche et al. 2011), APOGEE-1 (Majewski et al. 2015), UCAC4 (Zacharias et al. 2013), *Tycho-2* (Høg et al. 2000), APASS-DR7 (Henden et al. 2009), ALLWISE point sources (Cutri et al. 2013), and Sloan Digital Sky Survey point sources (SDSS; Alam et al. 2015). Cross matches are done directly with 2MASS IDs when possible, otherwise via cone search with 1 arcsec search radius. The proper motions and parallaxes for *Tycho-2* stars from the *Gaia* DR1 catalog (de Bruijne 2012; Lindegren et al. 2016) have also been cross-matched using the 2MASS IDs provided in the *Gaia* source catalog, and the *Gaia* DR2 catalog will be cross-matched after its planned data release in 2018.

The extended source base catalog is a positional cross-match that merges the full 2MASS extended source catalog (Skrutskie et al. 2006) and SDSS extended source catalog (Alam et al. 2015) to create a list of $\sim 125 \times 10^6$ objects. This base catalog is then positionally cross-matched with the ALLWISE extended source catalog (Cutri et al. 2013) and merged with the point source and special object lists.

Specially curated lists of objects (see Appendix E), such as stars from *Hipparcos* (Perryman et al. 1997),

known M-dwarfs (e.g., Lépine & Gaidos 2011), open cluster targets, and any additional objects of interest, are added to the TIC and CTL. The stellar properties supplied by those special lists supersede the default values in the TIC and CTL (see Appendix E for details).

The full list of TIC objects is subjected to a set of algorithms to determine the astronomical and physical parameters for each object as outlined in § 2.2 and prioritized within the CTL as described in § 3.3. The full TIC includes $\sim 596 \times 10^6$ objects ($\sim 470 \times 10^6$ point sources, $\sim 125 \times 10^6$ extended sources, and $\sim 1 \times 10^6$ objects from the specially curated lists). The TIC is staged for public use on the MAST portal system at <https://mast.stsci.edu>. The current release notes for the TIC are provided in Appendix A.

2.2. Algorithms for calculated stellar parameters

2.2.1. TESS magnitudes

The most basic quantity required for every TIC object is its position and apparent magnitude in the TESS bandpass, which we represent as T .¹ We estimate T using a set of empirical relations developed from PHOENIX stellar atmosphere models (Husser et al. 2016) to convert the available catalog magnitudes and colors to T magnitudes. Because the relationships between T and other magnitudes for stars with low surface gravities ($\log g < 3.0$) and low metallicities ($[\text{Fe}/\text{H}] < -0.5$) can be quite different from those of near solar-metallicity dwarfs (which are the targets of greatest interest for TESS), the relations are strictly valid for $\log g > 3$ and $[\text{Fe}/\text{H}] > -0.5$, though they may sometimes be used outside these ranges, subject to larger errors. They also are not valid for the very coolest dwarf stars with $T_{\text{eff}} < 2800$ K.

For each of the color- T relations, we have opted to define a single polynomial relation. As a result the calibrated relationships have somewhat larger scatter than might otherwise be possible with a more complex relation, but the scatter is still usually smaller than the errors from the original photometric catalogs, and thus we believe it is a worthwhile tradeoff for the sake of simplicity. The effects of reddening on T are not currently included² but are expected to be implemented in future versions of the TIC, see § 4.3.6.

We first present the relations for point sources, next for extended objects, and finally we provide any ancillary relations we developed for calculating other magnitudes such as B and V . We note that while most of the magnitude calculations are based on 2MASS magnitudes, we exclude values from our calculations with the following 2MASS quality flags: X, U, F, E, D. For the point sources we report a set of preferred relations, in order of preference, followed by a set of fallback relations that we use for a small number of stars for which it is not possible to apply any of the preferred relations. Column 63 in the TIC specifies which relation was used for any given star (see Appendix A).

Point sources, preferred relations

The following relations are valid for stars with $-0.1 < J - K_S < 1.0$. In all cases the J and K_S magnitudes are taken from 2MASS.

- T from V , J , and K_S :

$$T = J + 0.00152 X^3 - 0.01862 X^2 + 0.38523 X + 0.0293,$$

where $X = V - K_S$ and the scatter of the calibration is 0.021 mag. In this relation, the V magnitude might be taken from APASS, or calculated from the Tycho-2 B magnitude (see below).

¹For a definition of the TESS bandpass and of the TESS photometric system, see Sullivan et al. (2015).

²Many of the high priority TESS targets will be relatively nearby, and should not experience much reddening.

- T from B_{ph} , J , and K_S , where B_{ph} is a photographic B magnitude (from 2MASS via USNO A2.0):

$$T = J + 0.00178 X^3 - 0.01780 X^2 + 0.31926 X + 0.0381,$$

where $X = B_{ph} - K_S$ and the scatter is 0.020 mag.

- T from B , J , and K_S , where B is a Johnson magnitude:

$$T = J + 0.00226 X^3 - 0.02313 X^2 + 0.29688 X + 0.0407,$$

where $X = B - K_S$ and the scatter is 0.031 mag. In this relation, the B magnitude might be taken from any of several catalogs.

- T from J and K_S (for $J - K_S \leq 0.70$):

$$T = J + 1.22163 X^3 - 1.74299 X^2 + 1.89115 X + 0.0563,$$

where $X = J - K_S$ and the scatter is 0.080 mag.

- T from J , and K_S (for $J - K_S > 0.70$):

$$T = J - 269.372 X^3 + 668.453 X^2 - 545.64 X + 147.811,$$

where $X = J - K_S$ and the scatter is 0.17 mag.

- T from G and J , where G is the *Gaia* magnitude:

$$T = G + 0.00106 X^3 + 0.01278 X^2 - 0.46022 X + 0.0211,$$

where $X = G - J$. The scatter of this calibration is 0.015 mag. This relation will be updated should any updates to the *Gaia* passband be announced.

Point sources, fallback relations

There are some stars for which the $J - K_S$ colors are too blue or too red to determine a reliable T from the above relations. For these stars we use:

- T for $J - K_S > 1.0$:

$$T = J + 1.75 \quad (\pm 1.0 \text{ mag}).$$

- T for $J - K_S < -0.1$:

$$T = J + 0.5 \quad (\pm 0.8 \text{ mag}).$$

For a small subset of point sources in the TIC we have only a few magnitudes listed with passing quality flags from the available catalogs. For these, we adopt the following relations, if needed.

- T from V , J , and H (no K_S available):

$$T = V - 0.28408 X^3 + 0.75955 X^2 - 1.96827 X - 0.1140$$

where $X = J - H$, and the scatter is 0.063 mag.

- T from J , and H (no V or K_S available):

$$T = J - 0.99995 X^3 - 1.49220 X^2 + 1.93384 X + 0.1561$$

where $X = J - H$, and the scatter is 0.040 mag.

Finally, for faint stars for which only one magnitude is valid, the best we can do to compute T is to apply a simple offset from the one available magnitude. We wish to estimate a T magnitude in these cases, even if only crudely, because we wish to include all known objects in the sky as part of our flux contamination calculations (see Section 3.2.3). Because we rely on a specialty cool-dwarf catalog to identify faint, cool objects that are known to be *bona fide* M dwarfs, here we use models to compute T only for $T_{\text{eff}} > 3840$ K:

$$T = V - 0.6 \quad (\pm 0.9 \text{ mag}),$$

$$T = J + 0.5 \quad (\pm 0.8 \text{ mag}),$$

$$T = H + 0.7 \quad (\pm 1.3 \text{ mag}),$$

$$T = K_S + 0.8 \quad (\pm 1.4 \text{ mag}).$$

The uncertainties are representative of the spread for a range of T_{eff} , and the numerical value is an average.

Extended objects

- T from J , H , and K_S , relation valid for $J - K_S \leq 0.70$:

$$T = J + 1.22163 X^3 - 1.74299 X^2 + 1.89115 X + 0.0563,$$

where $X = J - K_S$ and the scatter is 0.008 mag. For the complementary color range $J - K_S > 0.70$ the relation is

$$T = J - 269.372 X^3 + 668.453 X^2 - 545.64 X + 147.811,$$

in which again $X = J - K_S$ and the scatter is 0.17 mag. It should be noted that since these relations were derived from models for dwarf stars, when applied to extended objects the errors will typically be larger than the formal scatter.

- T from SDSS g and i :

$$T = i - 0.00206 X^3 - 0.02370 X^2 + 0.00573 X - 0.3078,$$

where $X = g - i$ and the scatter is 0.030 mag.

If an SDSS extended source was found to have an unreasonable T magnitude³, then if $g = 30$, signifying a failure in measuring an SDSS magnitude, and *not* $i = 30$, we adopt $T = i - 0.5$ (± 1.0 mag). If $g \neq 30$ and $i = 30$, then we adopt $T = g - 1$ (± 1.0 mag).

Regarding the uncertainties in the TESS magnitudes, we have investigated the use of the full covariance matrix but it turns out those errors are typically small compared to the scatter of the calibration. Thus we believe it is more conservative to simply use the scatters provided above, added in quadrature to the errors propagated from the photometric uncertainties.

In a few cases where we are unable to calculate T we arbitrarily assign a value of $T = 25$. This is only the case for 1,725 objects in the TIC.

V magnitudes

In addition to T , we calculate a V magnitude for stars that do not have one in an existing catalog. We use the following relations depending on what magnitude information is available for each star. The total

³Typically an unreasonable T means $T < -5$ or $T > 25$

number of stars without reliable V magnitudes is expected to be small for CTL stars, but high for fainter stars in the TIC, and in any event we do not use these calculated V magnitudes for any of the physical parameter derivations described below (e.g., T_{eff} , dereddening, etc.). These relations are also mostly useful for dwarf stars, and are strictly valid for stars with $\log g > 3.0$. They are expected to give larger errors for metal-poor stars with $[\text{Fe}/\text{H}] < -0.5$ and for very cool dwarfs with $T_{\text{eff}} < 2800$ K.

- V magnitude from B_{ph} and K_S , where B_{ph} is photographic (from 2MASS via USNO A2.0):

$$V = J - 0.00814 X^3 - 0.03725 X^2 + 0.63921 X + 0.0323,$$

where $X = B_{ph} - K_S$ and the scatter is 0.023 mag. In this relation, the B magnitude might be taken from any of several catalogs.

- V from B and K_S , where B is a Johnson magnitude:

$$V = J + 0.00740 X^3 - 0.03897 X^2 + 0.57069 X + 0.0355,$$

where $X = B - K_S$ and the scatter is 0.041 mag. In this relation, the B magnitude might be taken from any of several catalogs.

- V from J and K_S :

$$V = J + 1.28609 X^3 - 2.35587 X^2 + 3.70190 X + 0.0766,$$

where $X = J - K_S$, the range of validity is $J - K_S \leq 0.70$, and the scatter is 0.027 mag. For the complementary color range $J - K_S > 0.70$ the relation is

$$V = J + 63.3104 X^2 - 86.2252 X + 31.1658.$$

The scatter of this relation is large (0.49 mag) so its usefulness is limited, but provided for completeness.

B magnitudes

Johnson B magnitudes are calculated for populating the B magnitude column of the TIC and for ensuring all magnitudes provided in the TIC are on the same photometric system, similar to what is done for the V magnitude calculations above.

- Johnson B magnitude from photographic B_{ph} and J :

$$J = B_{ph} - 0.00526 X^3 + 0.03256 X^2 + 0.14101 X - 0.0149,$$

where $X = B_{ph} - J$. While the overall scatter of the calibration is 0.060 mag, it is better for small X and much worse for large X . Therefore, when propagating errors and adding the scatter of the calibration in quadrature, 0.035 mag should be added to the scatter if $X < 3.5$, and 0.16 mag if $X > 3.5$.

The photometric errors for photographic magnitudes in 2MASS come from the USNO-A2.0 catalog. Based on that catalog's description⁴ the errors in the photographic B magnitudes are expected to be ~ 0.3 mag in the equatorial north and ~ 0.5 mag in the equatorial south.

2.2.2. Effective Temperature

Some stars in the TIC have spectroscopically derived T_{eff} values in the literature, and we use these where available⁵. Specifically, we have ingested several large spectroscopic catalogs, and we adopt the spectroscopic

⁴<http://vizier.u-strasbg.fr/vizier/VizieR/pmm/usno2.htx>

⁵See Appendix C for the providence flags

T_{eff} if the reported error is less than 300 K, giving preference to the catalogs in the priority order listed in Table 1. Additionally, the proper calculation of parameters such as T_{eff} for cool dwarf stars ($T_{\text{eff}} < 3840$ K) is typically very difficult when using ensemble dwarf relations, like we do in this section. Therefore, a specialized cool dwarf list was created to calculate these parameters. A brief explanation of the techniques used are described in § E.1.1 but we direct the reader to Muirhead et al. (2017, in prep) for more details.

Name	Data Release	Approximate Num. of Stars	Priority	Reference
SPOCS		1.6 k	1	Brewer et al. (2016)
PASTEL		93 k	2	Soubiran et al. (2016)
<i>Gaia</i> -ESO		29 k	3	Gilmore et al. (2012)
GALAH		10 k	4	Kordopatis et al. (2013)
APOGEE	DR-1	160 k	5	Majewski et al. (2015)
LAMOST	DR-1	120 k	6	Luo et al. (2015)
RAVE	DR-4	482 k	7	De Silva et al. (2015)
Geneva-Copenhagen	DR-3	16 k	8	Holmberg et al. (2009)

Table 1:: Spectroscopic Catalogs in the TIC.

However, the majority of TIC stars do not have spectroscopic T_{eff} values available. Therefore we have developed a procedure to estimate T_{eff} based on empirical relationships of stellar $V - K_S$ color. Because 2MASS is the base catalog for the TIC, we have a K_S magnitude for nearly every object (though to reiterate, we do not use 2MASS photometry whose quality flags are any of X, U, F, E, D). If a V magnitude is available from APASS (including the bright star extension), we adopt it unless $V < 7$; otherwise we adopt V_T from *Tycho-2*, or the V magnitude reported in the *Hipparcos* catalog. Finally, if none of the above are available, we adopt the aperture (CCD-based) magnitudes listed in the UCAC4 catalog (which are not far from Johnson V), unless they were flagged as unreliable (i.e., if the ‘number of images’ used is reported as zero). In all cases, we convert the adopted V magnitudes to Johnson V using standard conversion relations. In the case of the UCAC4 aperture magnitudes there appears to be no published conversion to Johnson V , so we developed our own, shown in Figure 2, based on $\sim 40,000$ stars that we cross-matched between UCAC4, APASS, and 2MASS.

The relation *for stars that are not identified as giants* (see Section 2.2.3) is in two pieces:

1. For $V - K_S$ in the range $[-0.10, +5.05]$ and $[\text{Fe}/\text{H}]$ in the range $[-0.9, +0.4]$, we use the AFGKM relation from Huang et al. (2015), assuming $[\text{Fe}/\text{H}] = 0$ if not available:

$$\begin{aligned}
 X &= V - K_S, Y = [\text{Fe}/\text{H}] \\
 \theta &= 0.54042 + 0.23676 X - 0.00796 X^2 - 0.03798 X Y + 0.05413 Y - 0.00448 Y^2 \\
 T_{\text{eff}}[\text{K}] &= 5040/\theta
 \end{aligned}$$

The scatter of this calibration is 2% in T_{eff} (Huang et al. 2015), which should be added in quadrature to whatever errors come from photometric uncertainties propagated through the above equation.

2. For redder $V - K_S$ values in the range $[5.05, +8.468]$, we use the relation from Casagrande et al. (2008), shifted by +205.26 K to meet with the one above at $V - K_S = 5.05$

$$\begin{aligned}
 X &= V - K_S \\
 \theta &= -0.4809 + 0.8009 X - 0.1039 X^2 + 0.0056 X^3 \\
 T_{\text{eff}}[\text{K}] &= 5040/\theta + 205.26
 \end{aligned}$$

The scatter of this calibration is only 19 K (Casagrande et al. 2008), which should be added in quadrature to the T_{eff} error from the photometric uncertainties as propagated through the above

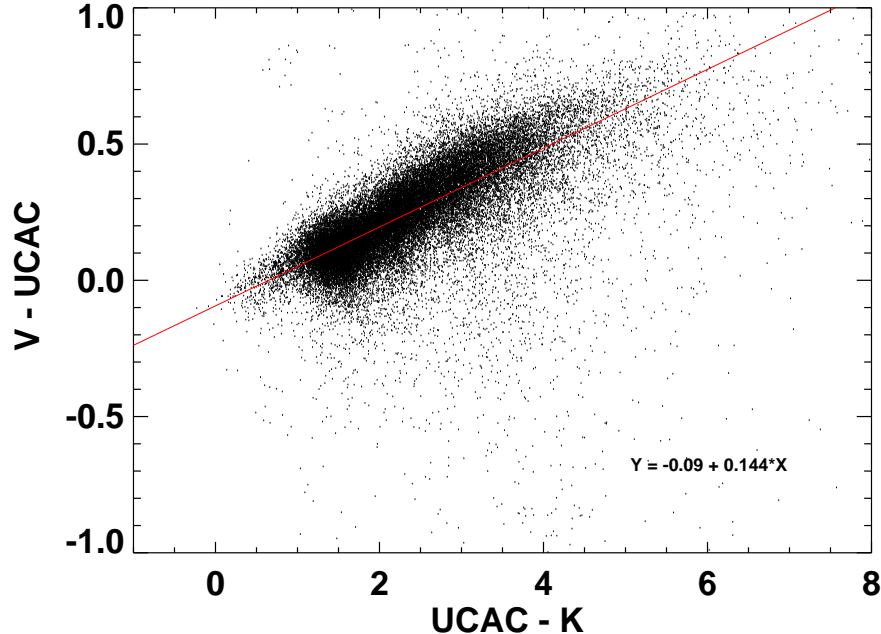


Fig. 2.— Determination of Johnson V from UCAC4 (near- V) aperture magnitudes as a function of the measured $V - K_S$ color from UCAC4 (using near- V for the color). Shown is the fit relation (red) to $\sim 40,000$ stars from a cross-match between UCAC4, APASS, and 2MASS.

equation. Note that this relation does not include metallicity terms, but Casagrande et al. (2008) claim that the dependence on metallicity is weak for $T_{\text{eff}} > 2800$ K.

Color-temperature relations can be challenging at cool T_{eff} because of the complexities of the spectral energy distributions of very cool stars. To validate the above relations at cool T_{eff} , we compared the T_{eff} predicted by the relation to the T_{eff} supplied independently by the specially curated Cool Dwarf list in the CTL (see Section E). The result of this comparison (Figure 3) indicates good agreement with no obvious systematics, except perhaps at the very coolest T_{eff} ($V - K_S \approx 7$, $T_{\text{eff}} \lesssim 2600$ K).

Finally, for completeness, we provide a similar relation for red giants, also from Huang et al. (2015):

$$\begin{aligned}
 X &= V - K_S, Y = [\text{Fe}/\text{H}] \\
 \theta &= 0.46447 + 0.30156 X - 0.01918 X^2 - 0.02526 X Y + 0.06132 Y - 0.04036 Y^2 \\
 T_{\text{eff}}[\text{K}] &= 5040/\theta
 \end{aligned}$$

which is valid for $V - K_S$ in the range [1.99, 6.09] and $[\text{Fe}/\text{H}]$ in the range $[-0.6, +0.3]$. The scatter in T_{eff} is 1.7% (Huang et al. 2015).

The above expressions provide a continuous color-temperature relation from 2444 K to 9755 K. For stars with $V - K_S$ outside of the above ranges of validity, the TIC reports $T_{\text{eff}} = \text{Nu11}$. For stars that are deemed to be likely non-giants according to our reduced-proper-motion procedure (see Section 2.2.3), the T_{eff} is calculated with the above relations but using the *de-reddened* $V - K_S$ color (see Section 3.2.1 for the de-reddening procedure). In general we *do not* calculate the T_{eff} for giants using a *de-reddened* color because we only apply our de-reddening procedure for stars identified as dwarfs which are the stars most likely to be included in the transit candidate targeting list (see Section 3). We note, finally, that in order to be conservative the final temperature errors from the above polynomial relations include a 150 K contribution added in quadrature to the uncertainties from the photometric errors and the scatter of the calibrations.

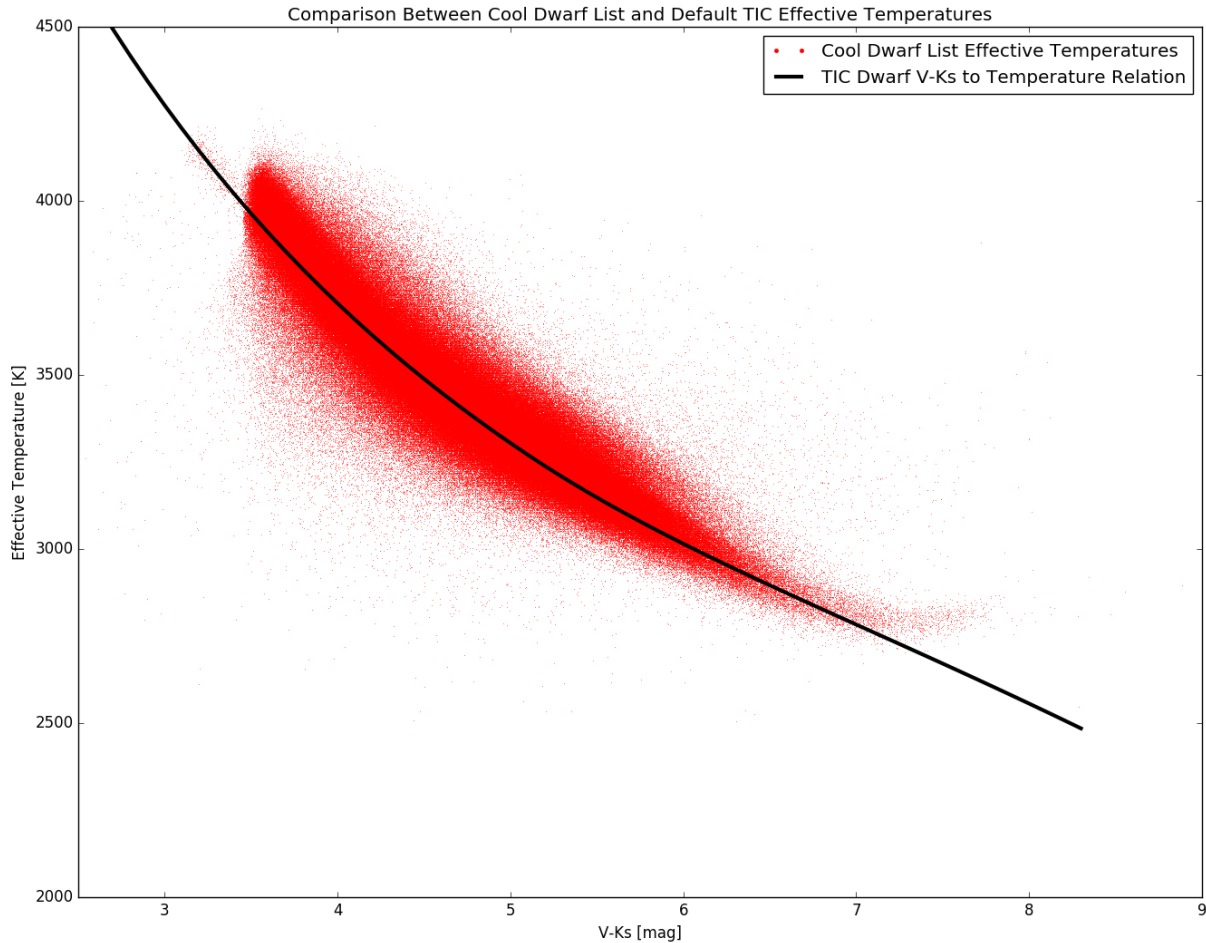


Fig. 3.— Plot of $V - K_S$ and T_{eff} of the independently determined T_{eff} for stars in the cool dwarf list (red dots) with the over plotted color- T_{eff} relation for dwarfs (black curve).

Confirmation of T_{eff} for cool dwarfs

Cool stars such as M dwarfs are a particularly important and valuable subset of TIC stars. To verify the T_{eff} that we determine for such stars, which will in turn affect the inferred stellar radii (see below), we compared our calculated T_{eff} with the values curated in the special Cool Dwarf list (see Section E). As shown in Figure 3, the independently determined T_{eff} from the Cool Dwarf list closely follows the color-based T_{eff} relation described above and we find a mean difference of only -19 ± 63 K.

2.2.3. Red giant removal

A key step for TESS targeting is the elimination of likely red giant stars, whose very large radii would make detection of transits by Earth-size planets very difficult. A visual overview of our methodology for removing likely giants is shown in Figure 4.

As indicated in Figure 4, when proper motion measurements are available we use the J -band reduced proper motion diagnostic ($\text{RPM}_J \equiv J + 5 \log \mu$, where μ is the total proper motion in arcsec yr^{-1}), adopting a slightly modified boundary from that proposed by Collier Cameron et al. (2007) to differentiate among

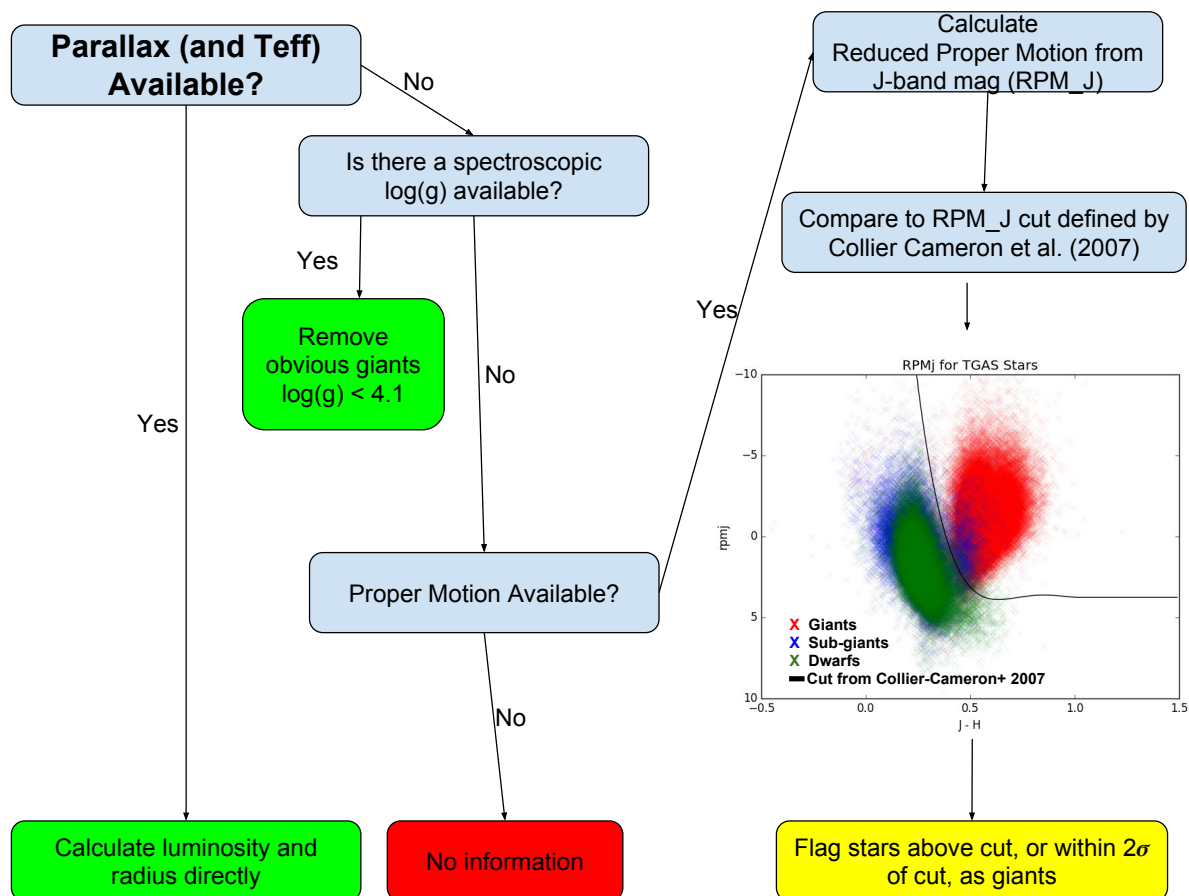


Fig. 4.— Overview of procedure for eliminating likely red giants from the TESS target sample. The inset uses *Gaia* DR1 stars to show the effectiveness of separating red giants (red points) in the RPM_J diagram using the cut defined by Collier Cameron et al. (2007). To the left/below the dividing line are dwarfs and subgiants; the RPM_J cut removes $\gtrsim 95\%$ of red giants but removes only $\sim 10\%$ of subgiants (see the text).

dwarfs ($\log g \gtrsim 4.1$), subgiants ($3.5 \lesssim \log g \lesssim 4.1$), and giants ($\log g \lesssim 3.5$). We define the boundary by the following polynomial relation:

$$RPM_{J,cut} \equiv -58 + 313.42(J - H) - 583.6(J - H)^2 + 473.18(J - H)^3 - 141.25(J - H)^4$$

for $J - H \leq 1$, and $RPM_{J,cut} \equiv 3.75$ for $J - H > 1$, such that stars at smaller (more negative) RPM_J values than the relation are considered to be giants, and those at larger (more positive) RPM_J values are considered to be dwarfs/subgiants.

If entries in multiple proper motion catalogs are available for a given star, we prioritize the proper motion measurements giving preference to those from the *Tycho-Gaia* Astrometric Solution (hereafter TGAS; Lindegren et al. 2016), then SUPERBLINK (Lépine & Gaidos 2011), then *Tycho-2*, then *Hipparcos*, and finally the UCAC4 catalog. We have chosen to rank *Tycho-2* above *Hipparcos* and UCAC4 because it has a significantly longer time baseline that can help to identify and remove binary motion contamination. SUPERBLINK was ranked above *Tycho-2* and *Hipparcos* because it incorporates a similar ranking for the priority of proper motions using *Tycho-2* and *Hipparcos*.

We tested the efficacy of the RPM_J method using stars with valid proper motion measurements and

independently measured $\log g$ from the spectroscopic catalogs in the TIC (see Section 2.2.2). We checked the degree to which the RPM_J cut correctly classified the stars according to their spectroscopic $\log g$. The results are shown as an inset in Figure 4 for $\sim 160,000$ stars with proper motions from *Gaia* DR1. We find that 2% of dwarfs are misidentified by the RPM_J method as giants, 4% of giants are misidentified as dwarfs, and 88% of subgiants are misidentified as dwarfs; thus the contamination of apparent giants by actual dwarfs is 1%, the contamination of apparent dwarfs by actual giants is 3%, and the contamination of apparent dwarfs by actual subgiants is 53%.

We also show these misidentification and contamination fractions as a function of Galactic latitude in Figure 5. There is a mild trend (note the vertical axes are logarithmic) for the misidentification of giants as dwarfs to be larger at high Galactic latitudes, reaching $\sim 10\%$ at the Galactic poles. The origin of this trend is not entirely clear, but is likely due to the very small number of giants with spectroscopic $\log g$ at high Galactic latitudes. Again, the fraction of giants misidentified as dwarfs *overall* is 4%.

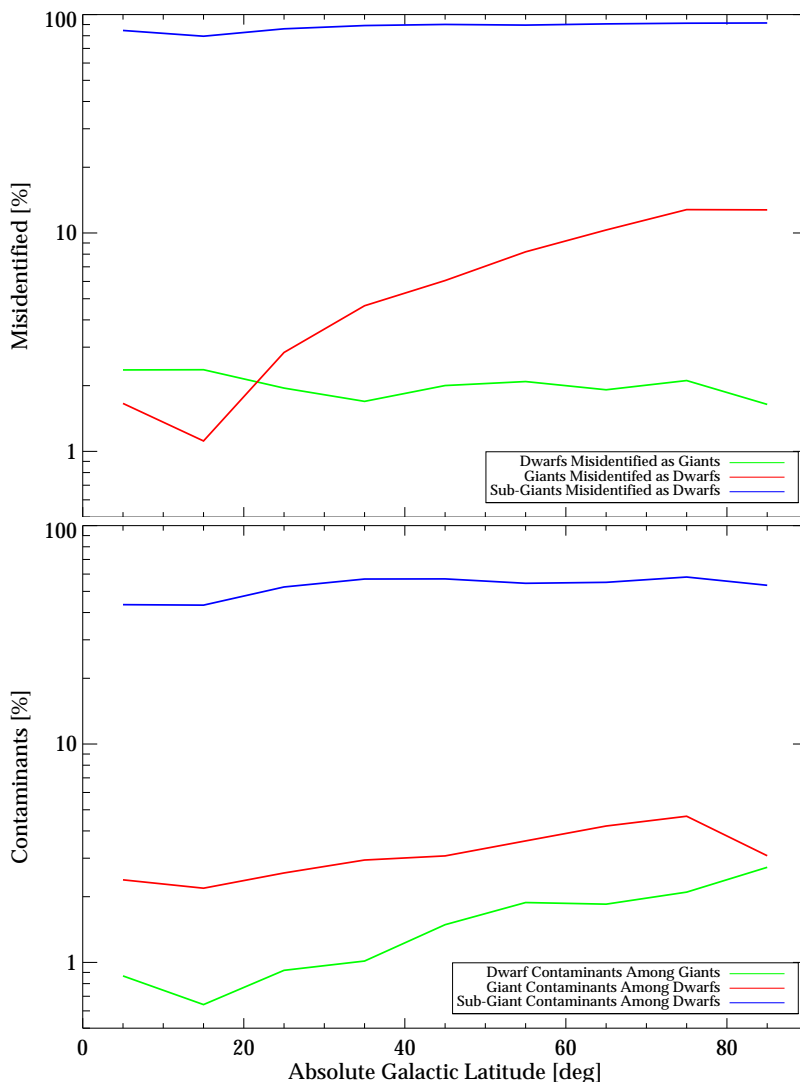


Fig. 5.— RPM_J misidentification and contamination rates among *Gaia* DR1 stars with spectroscopic $\log g$. (*Top:*) The fractions of dwarfs, subgiants, giants misidentified as other types, as a function of Galactic latitude. The apparent increase of giants misidentified as dwarfs may be due to the small number of giants toward the Galactic poles. (*Bottom:*) The fractions of dwarfs, subgiants, giants contaminating the others.

In any event, the RPM_J method is evidently able to remove red giants from the candidate dwarf sample with very high fidelity, but at the same time leaves a very high contamination of the candidate dwarf sample by subgiants of approximately 50%. Thus, subgiants remain as major contaminants among the putative dwarf sample. (See, e.g., Bastien et al. 2014, for a discussion of the reasons for this in the context of the bright *Kepler* sample.) In subsequent versions of the TIC we plan to use the *Gaia* parallaxes to screen out subgiants according to their radii (see, e.g., Stassun et al. 2017), for those stars that have parallaxes available. Finally, we checked that reddening in the RPM_J diagram does not adversely affect our ability to screen out likely red giants (Figure 6).

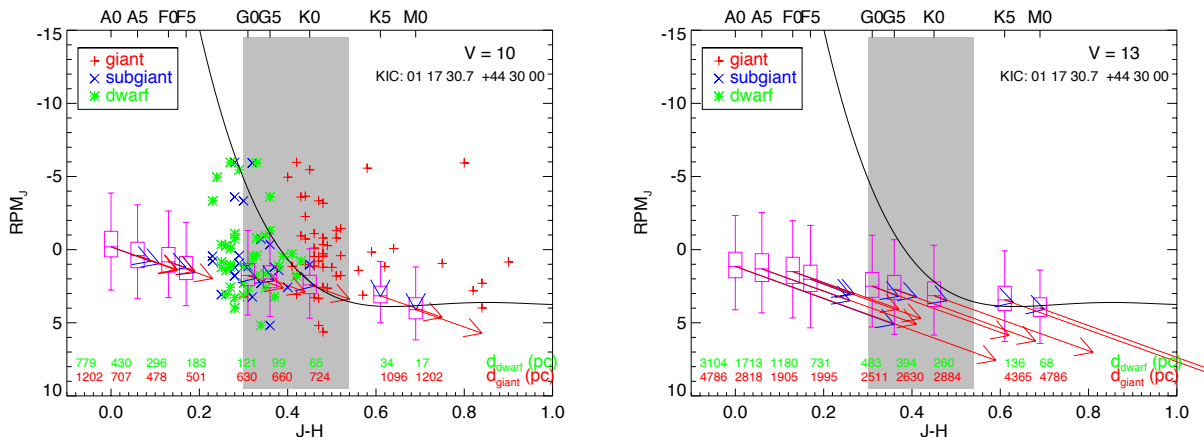


Fig. 6.— Effects of reddening on stars in the RPM_J diagram. Reproduced from Paegert et al. (2015). Reddening vectors are shown (in this case for the direction of the *Kepler* field) for representative stars. Reddening can shift some hot dwarfs into the red giant region (thus making them false-positive giants) but it is very unlikely for a red giant to be shifted into the dwarf region.

Validation of RPM_J M-dwarf selection with the Cool Dwarf List

As we did above with T_{eff} , we verified using the special Cool Dwarf list that our RPM_J method is reliable for the high-value M dwarfs. The TIC recovers more than 99% of these curated cool dwarfs, suggesting a high level of completeness for this subset of stars in the TIC. We also checked our calculated T and T_{eff} values for these stars against those supplied in the Cool Dwarf list (Figure 7), finding an r.m.s. difference in T of ~ 0.12 mag and in T_{eff} of ~ 63 K.

3. The Candidate Target List (CTL)

The purpose of the CTL is to provide a subset of TIC objects that can be used to select the target stars for TESS 2-min cadence observations (will most likely be as many as $\sim 400,000$) in service of the TESS mission’s primary science requirements, which are:

1. To search over 200,000 stars to detect planets with orbital periods less than 10 d and radii smaller than $2.5 R_{\oplus}$
2. To search for transiting planets with radii smaller than $2.5 R_{\oplus}$ and with orbital periods up to 120 d among 10,000 stars in the ecliptic pole regions.
3. To determine masses for at least 50 planets with radii smaller than $4 R_{\oplus}$.

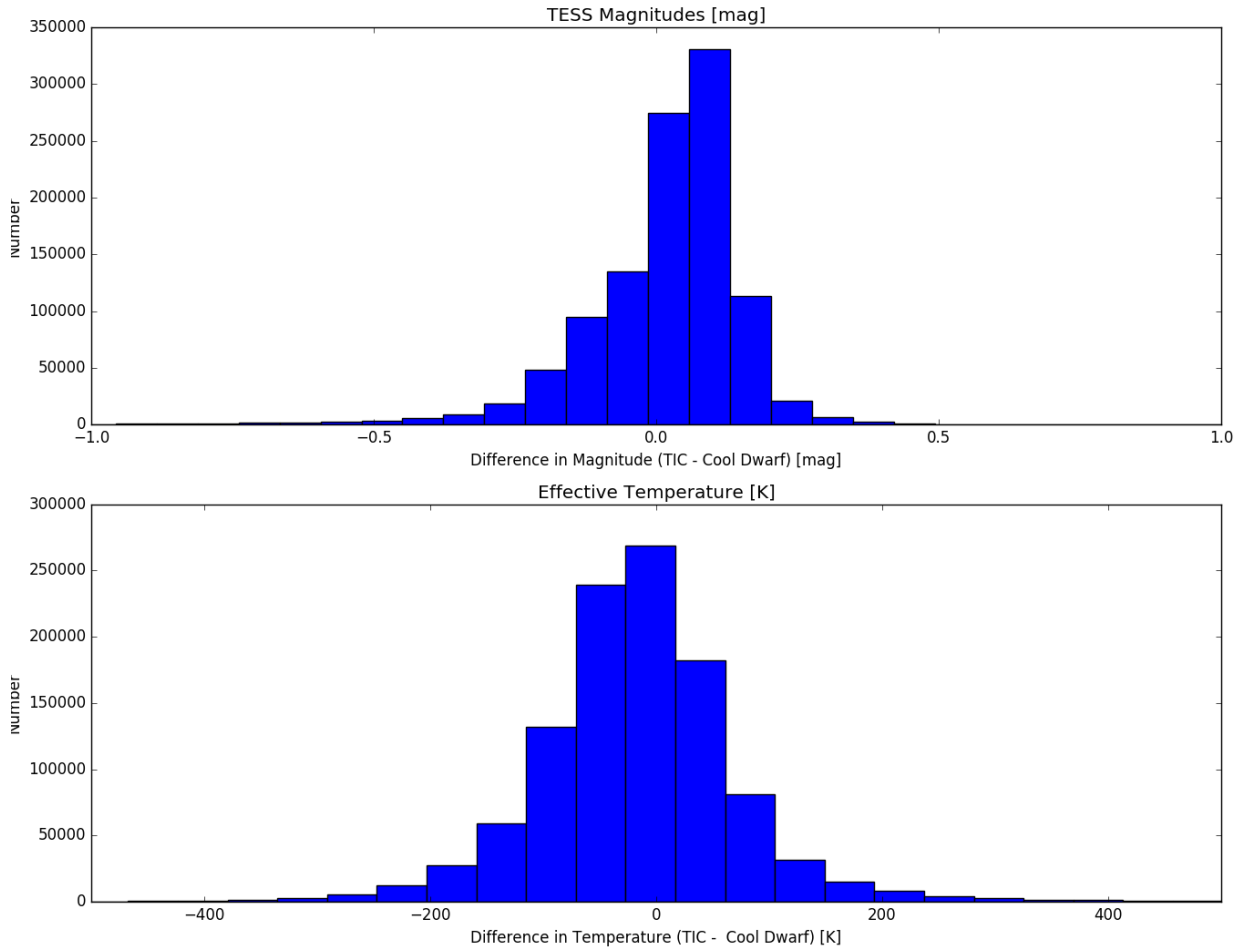


Fig. 7.— Comparison of calculated TESS magnitudes and T_{eff} for stars in the SUPERBLINK catalog known to be cool dwarfs ($T_{\text{eff}} < 4200$ K). We recover 99% of the stars as dwarf stars. Their spread in the predicted TESS magnitudes is ~ 0.12 mags, while the spread in the predicted T_{eff} is ~ 63 K.

Given the limited number of stars for which TESS will be able to acquire 2-min cadence light curves, it is crucial that the set of targets for TESS be optimized for small planet detection. To that end, we have compiled a catalog of bright stars that are likely to be dwarfs across the sky, from which a final target list for TESS can be drawn, based on in-flight observation constraints yet to be determined. This list of high-priority candidate 2-min cadence targets is the Candidate Target List (CTL). Our basic consideration is to assemble a list of dwarf stars all over the sky in the temperature range of interest to TESS, bright enough for TESS to observe, and taking extra steps to include the scientifically valuable M dwarfs. Our overall approach is to start with the 470 million stars in the TIC, and then apply cuts to select stars of the desired ranges in apparent magnitude and spectral type, and to eliminate evolved stars.

First, we give a brief overview describing the assembly of the CTL from the TIC. Next we describe the algorithms by which a number of stellar properties—such as stellar mass and radius—are computed for the CTL (Section 3.2). Finally, we present the prioritization scheme used for identifying the top priority targets from the CTL for targeting (Section 3.3). The CTL is provided for use through the Mikulski Archive for Space Telescopes (hereafter, MAST) and for interactive use via the Filtergraph data visualization system (Burger et al. 2013) at http://filtergraph.vanderbilt.edu/tess_ctl. A summary of the quantities included in the CTL on the Filtergraph portal is provided in Appendix F.

3.1. Assembly of the CTL

The application of cuts to the overall TIC to produce the CTL proceeds as follows with the approximate star counts for each step. From the 470 million point sources in the TIC we select the 76 million stars with $T < 15$. After then applying the RPM_J cut, we eliminate ~ 45 million as likely giants (this includes stars that are conservatively removed due to being within 2σ of the RPM_J boundary). Some 800,000 objects are removed for not having an available T_{eff} (due to poor photometry or no entry in the spectroscopic catalogs), no calculated radius (because of no available T_{eff}) and/or no calculated contamination ratio. These objects were removed because the priority depends on the radius and contamination ratio. We are left with about 31 million reasonably bright stars that are dwarfs or subgiants, and reliable effective temperatures. In order to further reduce that to a more manageable number for further analysis and prioritization, we remove ~ 20 million stars that are both relatively warm $T_{\text{eff}} > 5500$ K and faint $T > 12$, and unlikely to be high-priority targets for TESS.

The final set of stars comprises the CTL, with 10.8 million members. *We emphasize that at the present time—and until the Gaia DR2 parallaxes become available—the CTL includes both dwarfs and subgiants (see Section 2.2.3).*

As previously stated, we provide the CTL through the Filtergraph Portal system as a powerful tool for the astronomical community to interact with this unique data set. Since the Filtergraph system is not able to handle large numbers of users querying a dataset as large as the full CTL, we select only a subset of ~ 2.5 million stars to stage on the interactive portal. That subset consists of the CTL stars with the highest priority values, according to the prioritization metric described in § 3.3. Appendix F describes each quantity in the CTL that can be found on the Filtergraph Portal system.

3.2. Algorithms for calculated stellar parameters

3.2.1. Dereddening

Because we estimate stellar T_{eff} principally from empirical color relations, and especially because the favored relations involve the $V - K_S$ color (Section 2.2.2), which is highly susceptible to reddening effects, it is necessary to deredden the colors used for T_{eff} estimation, as we now describe.

Basic approach

Figure 8 (a reproduction of Figure 4 from Bessell & Brett 1988) shows that stars in the $V - K_S$ vs. $J - H$ color-color plane bifurcate between dwarfs and giants at $J - H \approx 0.7$. Any star with zero reddening should fall close to one of the two curves. Stars with reddened colors therefore will appear displaced from these curves along a reddening vector toward the upper right. Therefore, to *deredden* a star, we can move an observed star’s colors backward along the reddening vector until it falls on one of the two curves. Note that we update the relation from Bessell & Brett (1988), which used V with JHK to a relation that uses V with 2MASS JHK_S .

Reddening vector

We adopt a ratio of total-to-selective extinction of $R_V = 3.1$, and then calculate the corresponding extinctions in the near-IR colors (A_J, A_H, A_{K_S}) from Cardelli et al. (1989) to determine a unit reddening vector from the color excesses $E(V - K_S)$ and $E(J - H)$. These values allow us to define the direction of the dereddening vector, where the length of the vector is given by the usual reddening $E(B - V)$.

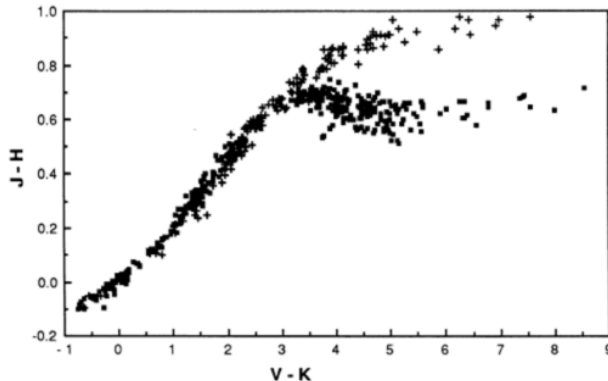


Fig. 8.— Reproduction of Figure 4 from Bessell & Brett (1988) showing the bifurcation of dwarfs (lower) and giants (upper) in the $J - H$ vs. $V - K$ color-color plane.

Dereddening procedure

We fit the dwarf and giant sequences from Bessell & Brett (1988) with polynomial functions (Figure 9, green and red curves, respectively), and divide the $V - K_S$ vs. $J - H$ plane into four regions.

For dwarf stars, the green line in Figure 9:

$$J - H = -0.048007 + 0.20983 X + 0.067020 X^2 - 0.036222 X^3 + 0.0049886 X^4 - 0.00021864 X^5$$

where $X = V - K_S$.

For giant stars, the red line in Figure 9:

$$J - H = -0.033479 + 0.18300 X + 0.040622 X^2 - 0.011824 X^3 + 0.00071399 X^4$$

where $X = V - K_S$.

Dereddening involves shifting the colors of a given star along the dereddening vector to one of the polynomial curves, or to a certain maximum if dereddening does not intersect one of the curves. Outside the Galactic plane ($|b| > 16^\circ$) we take $E(B - V)$ from the Schlegel et al. (1998) dust maps as the maximum, while within the Galactic Plane we arbitrarily adopt a maximum allowed $E(B - V) = 1.5$.

We consider stars in the four regions of the color-color plane in Fig. 9. In general, we shift the star along the dereddening vector until the star either: (i) intersects the dwarf sequence (green curve), or else (ii) we take the tip or tail of the vector, whichever lies closest to one of the (dwarf or giant) sequences. Specifically, we treat their dereddening as follows, using examples of stars in each region.

- Star A: No dereddening applied, as this would only move the star farther away from the dwarf sequence.
- Stars B and C: We shift the star along the dereddening vector until the star either: (i) intersects the dwarf sequence (green curve), or (ii) reaches the maximum dereddening (see above), or (iii) reaches closest approach to the dwarf sequence (magenta dashed line). Star B is typical for stars outside the Galactic plane that therefore have small reddening values. Star C is an example of a star in the plane for which we therefore adopt a maximum $E(B - V) = 1.5$ (see above); we adopt the point at which it intersects the dwarf sequence (marked by a dot).
- Stars D and E: We shift the stars along the dereddening vector until the star either: (i) intersects either the dwarf or giant sequence (green or red curve), or (ii) reaches the maximum possible dereddening, or

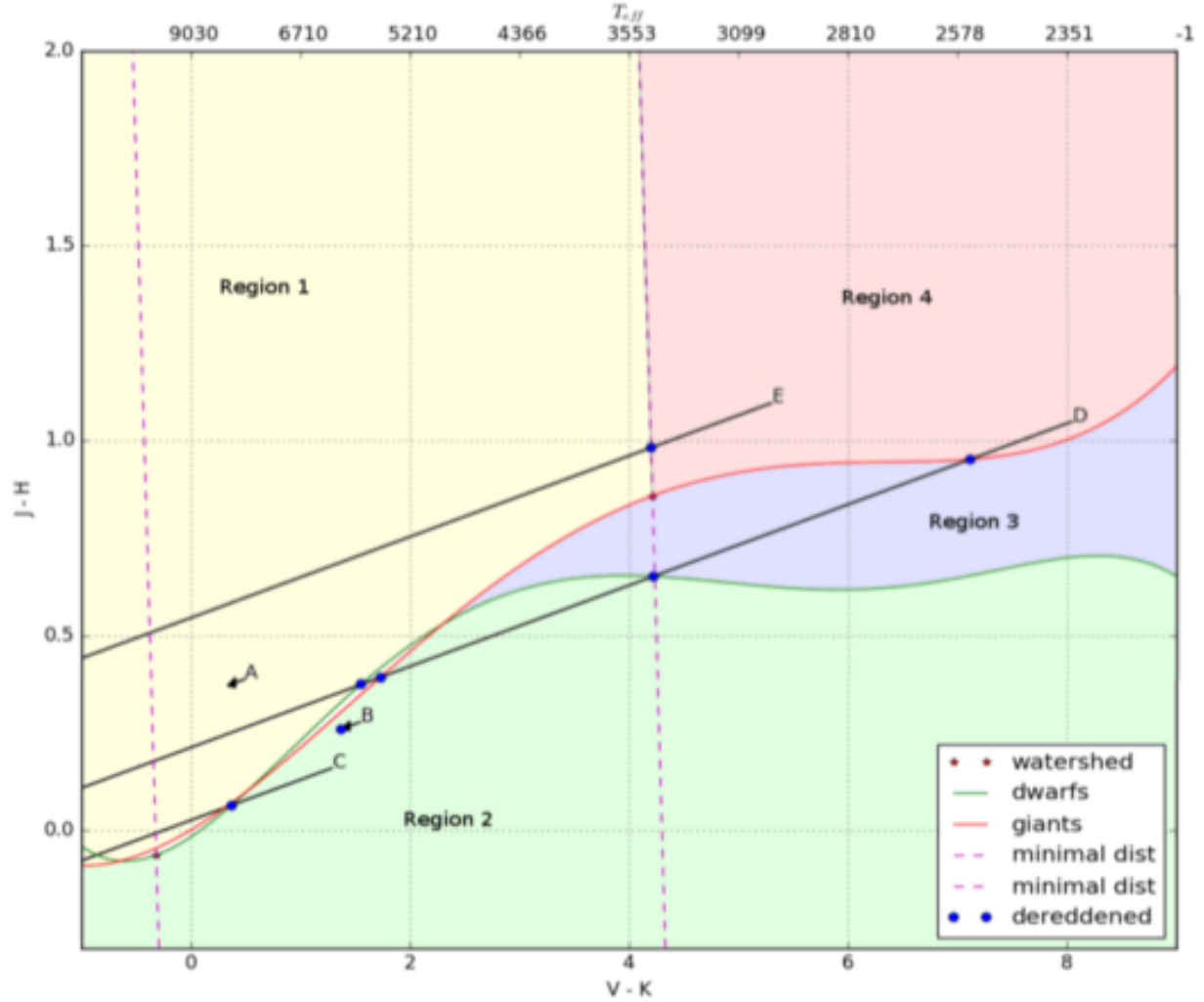


Fig. 9.— Illustration of dereddening for stars in different parts of the $J - H$ vs. $V - K_S$ color-color diagram.

(iii) reaches the closest approach to one of the sequences (magenta dashed lines). The vector for star D crosses the dwarf/giant sequences four times; in such cases we store all values (indicated by blue dots) but adopt the smallest reddening value. Star E is an example where the vector crosses neither the dwarf nor giant sequence; in these cases we instead adopt the value of the closest distance (magenta dashed line) between the dereddening vector and the giants sequence as indicated by the blue dot.

- For stars earlier than M-type ($V - K_S \leq 2.2241$) and within the typical $J - H$ error (0.05 mag) of the dwarf relation (green curve in Figure 9), we assume zero reddening. These stars have been flagged with ‘dered0’ in the CTL.

Once dereddened as described here, the colors are used to determine an updated T_{eff} following the procedures described in Section 2.2.2. In cases where the reddening cannot be determined (i.e., dereddening would move the star to a region of color space beyond the range of applicability of our color- T_{eff} relations), no dereddening is attempted and the star is flagged for exclusion from the CTL (see below).

We have compared our photometrically estimated T_{eff} values to the spectroscopically determined values from the LAMOST survey, as a general check on our T_{eff} estimates and as a specific check on the dereddening

procedure. We did this comparison for two different photometric dereddening techniques: (1) the scheme described above, and (2) using a 3D Galactic dust model from Bovy et al. (2016) through which we iteratively estimate the distance on the assumption that the star is a main-sequence star. The latter procedure was examined because the Schlegel et al. (1998) maps do not provide reliable maximum line-of-sight extinctions within 15° of the Galactic plane. Figure 10 shows the results of these comparisons for dwarfs, subgiants, and giants categorized according to the LAMOST spectroscopic $\log g$.

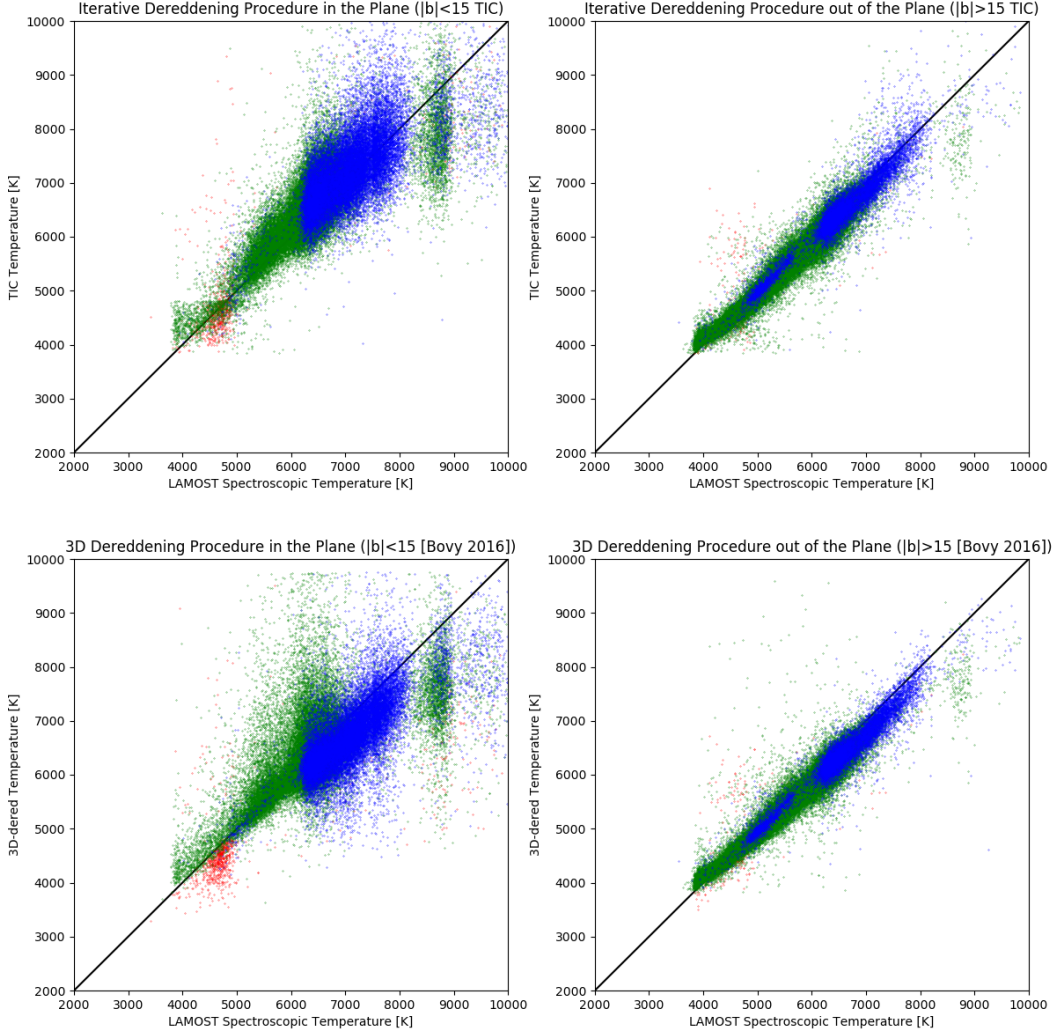


Fig. 10.— Comparison between our photometrically dereddened T_{eff} and LAMOST spectroscopic T_{eff} for dwarfs (green), subgiants (blue), and giants (red, there are only a few dozen green points). *Top:* The dereddened T_{eff} calculated as described in Section 3.2.1. *Bottom:* The dereddened T_{eff} calculated using the 3D dust maps of Bovy et al. (2016). We find the two methods to be comparable and thus adopt the method of moving stars in the $J - H$ vs. $V - K_S$ plane (Sec. 3.2.1) for computational expedience.

We find that the method of moving stars in the $J - H$ vs $V - K_S$ plane shows results similar to the 3D dereddening approach outside of the plane (differences relative to LAMOST of -64 ± 115 K, compared to -104 ± 119 K) and inside the plane (178 ± 370 K compared to -157 ± 337 K). This difference is not large, and because the computational effort required for the 3D approach is enormous for the ~ 11 million stars in the CTL, we adopt the method of dereddening the stars in the $J - H$ vs. $V - K_S$ plane.

3.2.2. Stellar Mass and Radius

In order to prioritize the stars based on the ability of TESS to observe transits by Earth-size planets (see Section 3.3), it is essential to estimate the stellar radii and masses. When available, we simply adopt the radii and masses from the specially curated catalogs (Appendix E), such as those provided in the Cool Dwarf list. These values are always accepted as the best representation of the true parameters and are given preference over any other values in the TIC. When such special catalog information is not available we use the procedures described below to calculate each parameter, in order of preference.

Stars with spectroscopic parameters

When spectroscopic T_{eff} and $\log g$ are available, we calculate mass and radius from empirical relations (Torres et al. 2010), with a reported scatter of 6.4% in mass and 3.2% in radius.

Stars with parallax but no spectroscopic parameters

If no spectroscopic information is available, but a parallax is available, we calculate the radius from the Stefan-Boltzmann equation, as follows. We first calculate the V -band bolometric correction, BC_V , using a polynomial formulation by Flower (1996), which is purely empirical and has been found to work reasonably well for solar-type and hotter stars. The coefficients for three different T_{eff} ranges are shown in Table 2 (see Torres 2010), where $\text{BC}_V = a + b \log T_{\text{eff}} + c (\log T_{\text{eff}})^2 + d (\log T_{\text{eff}})^3 + e (\log T_{\text{eff}})^4 + f (\log T_{\text{eff}})^5$. We add the following offsets to the above polynomial relations to make the three T_{eff} ranges meet smoothly: For $\log T_{\text{eff}} < 3.7$, add -0.022 mag to the polynomial result; for $3.7 \leq \log T_{\text{eff}} < 3.9$, no offset; and for $\log T_{\text{eff}} \geq 3.9$, add -0.003 mag to the polynomial result.

	Cool Regime $\log T_{\text{eff}} < 3.7$	Middle Regime $3.7 \leq \log T_{\text{eff}} < 3.9$	Hot Regime $\log T_{\text{eff}} \geq 3.9$
a	$-0.190537291496456\text{d}+05$	$-0.370510203809015\text{d}+05$	$-0.118115450538963\text{d}+06$
b	$+0.155144866764412\text{d}+05$	$+0.385672629965804\text{d}+05$	$+0.137145973583929\text{d}+06$
c	$-0.421278819301717\text{d}+04$	$-0.150651486316025\text{d}+05$	$-0.636233812100225\text{d}+05$
d	$+0.381476328422343\text{d}+03$	$+0.261724637119416\text{d}+04$	$+0.147412923562646\text{d}+05$
e	...	$-0.170623810323864\text{d}+03$	$-0.170587278406872\text{d}+04$
f	$+0.788731721804990\text{d}+02$

Table 2:: BC_V Relation Coefficients Adopted from Flower (1996).

With BC_V in hand, we next calculate the bolometric luminosity, L_{bol} , as follows:

1. Correct the apparent V magnitude for extinction (A_V): $V_0 = V - A_V$;
2. Calculate absolute V -band magnitude with: $M_V = V_0 - 10 + 5 \log \pi$, where π is the *Gaia* DR1 parallax in milli-arcseconds;
3. Compute the absolute bolometric magnitude with $M_{\text{bol}} = M_V + \text{BC}_V$;
4. Compute the bolometric luminosity in solar units with $\log L/L_{\odot} = -0.4(M_{\text{bol}} - M_{\text{bol},\odot})$, where $M_{\text{bol},\odot} \equiv 4.782$.⁶

⁶This is the value appropriate for the scale of the Flower (1996) bolometric corrections, such that the measured apparent

The final formula for L_{bol} is therefore: $\log L/L_{\odot} = -0.4(V - A_V - 10 + 5 \log \pi + \text{BC}_V - 4.782)$.

Finally, we calculate the radius from T_{eff} and the Stefan-Boltzmann law using $T_{\text{eff},\odot} \equiv 5772$ K, as recommended by the IAU (2016 Resolution B3). The above methodology is valid for $T_{\text{eff}} \geq 4100$ K. The stellar radii for cooler stars will be obtained using other methods, as described in § 3.2.2.

To compute the error in the radius we propagate the observational uncertainties for all of the above quantities. For the *Gaia* DR1 parallax the total error is the quadrature sum of the nominal uncertainty and 0.3 mas systematic error (Lindegren et al. 2016). For BC_V we have chosen to add 0.10 mag in quadrature to the BC_V uncertainty that comes from the T_{eff} error via the Flower (1996) polynomials. The error in $M_{\text{bol},\odot}$ is taken to be the estimated error in V_{\odot} , which is 0.02 mag. Stellar mass is discussed below.

Stars with neither spectroscopic parameters nor a parallax available

When none of the above sources of stellar radii are available, we determine the stellar radii as well as the masses using a single relation for each quantity based on T_{eff} . They were derived from high-precision empirical measurements of masses and radii of eclipsing binaries (Torres et al. 2010), which in the case of the radii show relatively little scatter for hot and cool stars, but a considerably larger scatter for intermediate-temperature stars where subgiants are more common. However, in this regime the sample of eclipsing binaries was found to be sparse, and was therefore supplemented with simulations based on the TRILEGAL code (Girardi et al. 2005) to generate a population of stars that is complete in both mass and radius at a given T_{eff} .

The TRILEGAL sample was created using 12 representative sight lines at a Galactic longitude of 90° and Galactic latitudes between 30° and 85° . Each sight line covered 10 deg^2 and excluded binaries, which led to $\sim 390,000$ objects brighter than $T = 20$. We included both dwarfs and subgiants, since these are the largest sample populations in the TIC.

We drew spline curves through the middle of the distribution of points in the mass-temperature and radius-temperature diagrams, and also along the upper and lower envelopes (considering both the eclipsing binaries and the simulated stars from TRILEGAL) so as to provide a means to quantify the mass and radius uncertainties from their spread. The nodal points of these spline functions are provided in Tables 3–4, and the final relations are shown in Figure 11.

In the range of T_{eff} occupied by significant numbers of subgiants, the asymmetric spread toward larger radii is very large, but then decreases sharply below about 4800 K (because for the age of the Milky Way, all stars at such cool T_{eff} are either main-sequence dwarfs of very low mass or else evolved red giants of higher mass). It was found convenient to split the upper envelope of the radius-temperature relation into two regimes at 4800 K, which introduces a discontinuity that matches what is seen in the TRILEGAL simulations. This is seen as well in Figure 11.

As discussed in Section 2.2.3, we find that our RPM_J -based procedure for removal of red giants does not effectively remove subgiants, and therefore the largest radius errors are for G-type stars, since there are large numbers of G subgiants. On the other hand, since there are no cool subgiants, typical radius errors for cool stars are small, reflecting only the small spread on the main sequence. Radius errors are also small for hotter stars (A and F types), as mentioned before, because massive subgiants evolve extremely quickly

visual magnitude of the Sun is reproduced exactly (Torres 2010). Note that the apparent visual magnitude of the Sun implicitly adopted here ($V_{\odot} = -26.71$) in order to derive $M_{\text{bol},\odot} = 4.782$ is the currently accepted value, and is different from the value of $V_{\odot} = -26.76$ adopted by Torres (2010). Note also that the value of $M_{\text{bol},\odot}$ above is not the same as the one recently defined by the IAU ($M_{\text{bol},\odot} = 4.75$; 2016 Resolution B2), because the Flower (1996) scale is not the same as the scale recently defined by the IAU. For TESS we must use $M_{\text{bol},\odot} = 4.782$, or there would be a systematic error when adopting the bolometric corrections from Flower (1996).

through the Hertzsprung gap and there are few blue giants in the local neighborhood. For the purposes of the TIC, which as defined permits only a single value for radius error or mass error, we are unable to supply asymmetric errors. Therefore, for the purposes of the TIC only, for the radius error we adopt the average of the upper and lower asymmetric errors from Table 3, capped at 100% of the radius, and for the mass error we report the average of the upper and lower errors from Table 4, which is always smaller than 100% of the mass.

Type	$T_{\text{eff}}[\text{K}]$	Mean Radius [R_{\odot}]	Lower Radius Limit [R_{\odot}]	Upper Radius Limit [R_{\odot}]
O5	42000	11	9.0	14.2
B0	30000	6.2	5.12	8.0
B5	15200	3	2.38	4.3
B8	11400	2.6	1.83	4.39
A0	9790	2.4	1.66	4.54
A5	8180	2.1	1.53	4.45
F0	7300	1.8	1.40	4.32
F5	6650	1.55	1.23	4.2
G0	5940	1.2	1.00	4.0
G5	5560	1.05	0.90	3.84
K0	5150	0.9	0.79	3.67
K2	0.889/3.4 ⁷
K5	4410	0.72	0.65	0.79
M0	3840	0.60	0.52	0.67
M2	3520	0.47	0.35	0.59
M5	3170	0.28	0.20	0.37

Table 3:: Nodal points of the T_{eff} -radius spline relations.

Type	$T_{\text{eff}}[\text{K}]$	Mean Mass [M_{\odot}]	Lower Mass Limit [M_{\odot}]	Upper Mass Limit [M_{\odot}]
O5	42000	40.0	36.0	44.0
B0	30000	15.0	13.5	17.0
..	22000	7.5	6.9	8.5
B5	15200	4.4	3.95	5.0
B8	11400	3.0	2.6	3.5
A0	9790	2.5	2.15	3.0
A5	8180	2.0	1.7	2.48
F0	7300	1.65	1.40	2.15
F5	6650	1.4	1.18	1.80
G0	5940	1.085	0.965	1.22
G5	5560	0.98	0.87	1.11
K0	5150	0.87	0.78	0.98
K5	4410	0.69	0.615	0.77
M0	3840	0.59	0.51	0.67
M2	3520	0.47	0.37	0.59
M5	3170	0.26	0.19	0.35

Table 4:: Nodal points of the T_{eff} -mass spline relations.

3.2.3. Flux contamination

If a TESS target is blended with a foreground or background star, the flux from the nearby source will fall into the TESS aperture of the target star, decreasing the ability to detect transits of the target. We use the catalogs described in Section 2.1 to identify all flux-contributing sources near each TESS target.

We identify all potential contaminants for each TESS target, down to the limiting magnitudes of APASS and 2MASS ($T \sim 17\text{--}19$), and we calculate the fraction of contaminating flux in the aperture for the TESS target. That calculation relies on three quantities: (1) the distance out to which a star might possibly

⁷At this spectral type there is a discontinuity in the upper radius limit. See Fig. 11 for details.

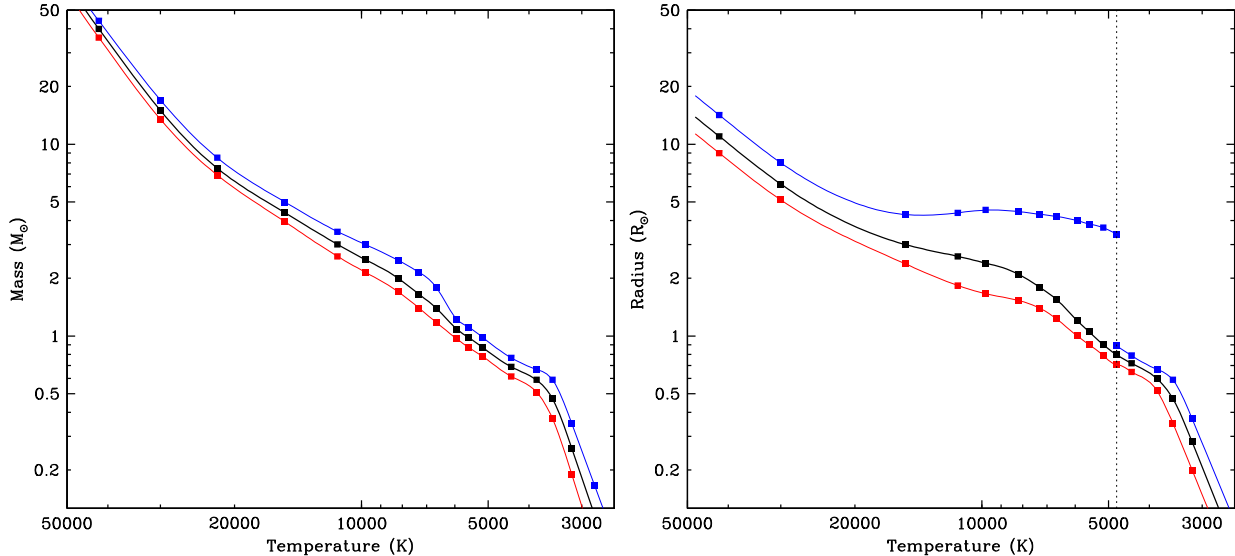


Fig. 11.— Derived mass- T_{eff} (left) and radius- T_{eff} (right) relations for the TIC based on a combination of eclipsing binary measurements of the mass and radius (Torres et al. 2010) and TRILEGAL simulations, to gain a more representative sample. The nodal points of the spline curves are given in Tables 3 and 4. In both figures the blue points are the upper mass/radius limits, the black points are the mean values, and the red points are the lower mass/radius limits. The vertical dotted line in the radius- T_{eff} diagram marks the break in the upper envelope at ~ 4800 K caused by larger subgiant stars hotward of that limit.

contaminate a target, (2) the shape and size of the TESS point-spread-function (PSF), and (3) the size of the TESS aperture.

In order to calculate expected contamination ratios for TESS targets before the mission launches in a computationally practical way, we make a set of assumptions for each of the quantities involved. For the maximum angular distance out to which a source might contribute contaminating flux, we adopt a distance of 10 TESS pixels. Although especially bright stars a larger distances will have wings of the their PSF at distances significantly larger than that, their density on the sky is small.

For the shape and size of the TESS PSF, we use a preliminary empirical PSF determined by the TESS mission. Although the small focal ratio of the TESS optics, means that there will be significant non-circularity and focal plane distortions in the TESS images, we will not know until TESS launch where a given target will fall in the TESS camera field. Therefore, we select the empirical TESS PSF determined for the center of the TESS field of view, which generally represents the most compact PSF, and therefore represents a lower limit of the rate of flux contamination for a given star.

We fit both a Moffat model and a 2D Gaussian model to the empirical PSF. While there is virtually no difference between the empirical PSF and both the Moffat and Gaussian models in integrated flux, the relative errors reveal that the Gaussian underestimates the total flux by 5%. However, because it does this both for the target and the nearby contaminating stars, the effect partially cancels out. The main difficulty with a 2D Moffat profile is that there is no analytical solution for the integral over the function, and we would have to integrate numerically which requires considerable computing resources. Therefore we select a circular 2D Gaussian model⁸ (see Fig. 12).

Just as the TESS PSF is not fully determined at this time, the size of the aperture used for a given

⁸The function used to calculate the PSF will be included as a tool for use by the Guest Investigator program.

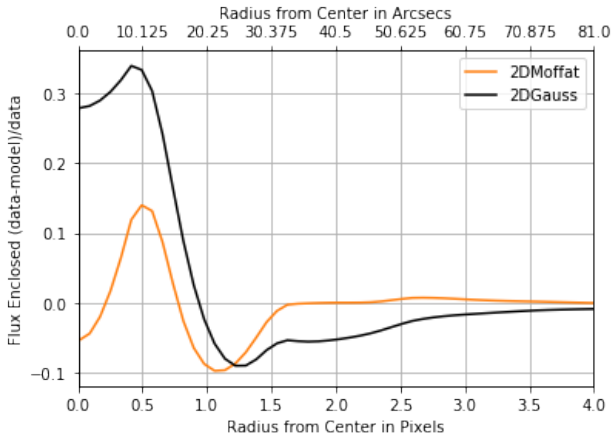


Fig. 12.— The difference in integrated fluxes between the preliminary TESS PSF and the 2D Gaussian and 2D Moffat models.

TESS target is not known precisely. As TESS prepares to observe each sector, the mission will define the set of pixels to be acquired for each 2-minute target. After those pixels are downloaded, the SPOC will determine the optimal pixels to be used from the downloaded pixel set for the mission-derived light curves. The size of the pixel set depends on the size and shape of the PSF, the brightness of the target star, the placement of the target stars in the TESS field, and the location of nearby objects.

For the analysis here, the size of the aperture is adaptive based on T of the star. We determine the radius of a circle around a given target for a given T , and then derive the side-length of an enclosing square and the side length of an area preserving square. Both are averaged and this average is the size of the aperture. We calculate a given star’s PSF using the formula below, requiring the PSF to be no smaller than 1 pixel and limiting the brightest stars to have a PSF size equal to that of a $T = 4$ star.

$$N_{\text{pix}} = c_3 T^3 + c_2 T^2 + c_1 T + c_0$$

where $c_3 = -0.2592$, $c_2 = 7.7410$, $c_1 = -77.7918$, and $c_0 = 274.2898$.

We calculate the contamination ratio as the ratio of flux from nearby objects that falls in the aperture of the target star, divided by the target star flux in the aperture. The nominal parameters we adopt for these calculations are as follows:

- Pixel size: 20.25 arcsec
- Contaminant search radius: 10 pixels
- Standard deviation for the 2D Gaussian model: $\text{FWHM}/(2\sqrt{2\ln 2})$.

The flux contamination for ~ 10 million stars in the CTL is shown in Figure 13.

3.3. Target prioritization

The overarching consideration for prioritization of TESS targets is the detectability of transits by small, rocky (i.e., Earth-size) planets. Therefore, the primary stellar parameters that factor into the prioritization scheme are (1) stellar radius (a given planet produces a deeper transit for a smaller star), and (2) stellar brightness (more photons detected translates to better ability to detect smaller transits).

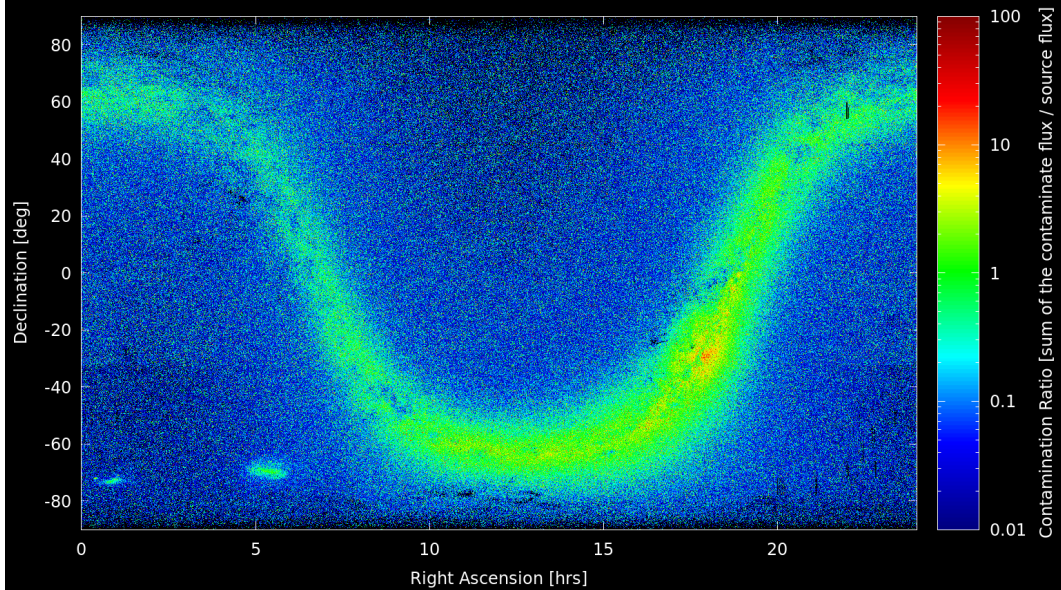


Fig. 13.— Estimated flux contamination ratio for stars in the CTL with contamination between 0.01 and 100. The contamination ratio clearly increases toward the Galactic plane and Magellanic Clouds.

More specifically, the signal-to-noise ratio (SNR) of a transit is $\sqrt{\Delta X^2}$, and $\Delta X^2 = N(d/\sigma)$, where d is the transit depth, N is the number of observations in transit, and σ is the per-point photometric error. Since $d = (R_p/R_\star)^2$, where R_p and R_\star are the planetary and stellar radii, respectively, then the minimum detectable planetary radius is $R_p \propto R_\star \sqrt{\sigma}$.

This approach is quite simplistic, and actually formally incorrect, since it takes a fiducial fixed depth transit, and ignores transit depth dependence on the planet size. It also assumes that we have no information about the planet orbital period, and thus no way to know how many in-transit points to expect, and a fixed ΔX^2 . It also ignores other factors that influence planet detectability. A more sophisticated approach is being developed for future versions of the CTL prior to TESS launch. This initial formulation is provided as a first pass at target prioritization, in anticipation of further scientific considerations for TESS science goals.

The value of the photometric error σ can be calculated directly from the T magnitude. For the calculation of σ as a function of T we adapt the following functional form (L. Bouma, private communication) based on the relationship provided in Figure 8 of Ricker et al. (2015) for I_C magnitudes⁹:

$$\ln \sigma[\text{ppm}] = \ln A + B T + C T^2 + D T^3 + E T^4 + F T^5$$

with the associated coefficients given by:

$$\begin{aligned} F &= +4.73508403525 \times 10^{-5} \\ E &= -0.0022308015894 \\ D &= +0.0395908321369 \\ C &= -0.285041632435 \\ B &= +0.850021465753 \\ \ln A &= +3.29685004771 \end{aligned}$$

⁹The I_C magnitude was originally used as a proxy for T in early analysis. For the purpose of our priority calculations we adopt the I_C formula as a sufficiently good approximation.

Note that we do not correct for extinction in this case because we wish to estimate the signal based on the actual observed brightness, and not the “intrinsic” brightness. However, we do still use the dereddened T_{eff} for estimating R_{\star} . We also include flux contamination into the prioritization scheme. The contamination ratio is defined as the total contamination flux in the aperture divided by the total flux from the source.

It is also the case that stars that are observed in more than one 27-day observing sector will be observed for additional time, gathering additional signal, and extending the orbital period range that can be probed by TESS. However, since we do not yet know the locations of the TESS sectors, for now we only modify the prioritization for targets that appear in the northern or southern TESS Continuous Viewing Zones (CVZs), specifically, targets north of ecliptic latitude $+78^{\circ}$ and south of ecliptic latitude -78° . Also, we only account for the additional SNR for such targets in terms of fiducial transit detection, and not the many other scientific considerations that apply to both longer dwell times on targets and also additional number of observations. Since the targets in the CVZs will be observed 13 times longer than most other targets, we boost their priorities by a factor of $\sqrt{13}$.

Finally, we de-prioritize objects within the Galactic plane ($|b| < 15$) by a factor of 0.1. We note this does not apply to stars with spectroscopic T_{eff} or are identified in special target lists. This is done to alleviate the tension caused when our poor understanding of the true reddening for stars in the plane causes the radius calculations, which are dependent on T_{eff} , to produce unphysically large values.

The final priority, therefore, is defined as:

$$\frac{\delta}{R_{\star} \sqrt{\sigma \times \sqrt{\epsilon + 1}}}$$

where δ is the CVZ boosting factor (either 1 if $|\beta| < 78^{\circ}$, or $\sqrt{13}$ if $|\beta| > 78^{\circ}$), R_{\star} is the stellar radius in solar radii, σ is the total photometric precision, and ϵ is the contamination ratio. We normalize the priority values by dividing by the smallest expected stellar radius ($0.1 R_{\odot}$), the smallest expected precision (61.75×10^{-6}), and the smallest possible contamination (0), all combined in the same way.

This normalized priority thus extends from 1 (highest priority) to 0 (lowest priority). Because of the deliberate boosting of the stars in the CVZs, a large fraction of the top priority stars in the CTL are preferentially located in those regions. Of the top 400,000 stars in the CTL, about 160,000 are located in the CVZs. Of the top 200,000 stars in the CTL, about 120,000 are located in the CVZs. Note that in these tabulations, we have not excluded the ecliptic plane region (which will not be observed by TESS during the nominal 2-year mission) so that we can provide all-sky considerations for the target star properties, which will become relevant if the TESS mission is extended and those observations cover the ecliptic region.

The very large fraction of TESS targets in the CVZs is a deliberate decision on our part. Furthermore, the degree of that overabundance is arguably even less that would be scientifically motivated. The exiting priority boost accounts for the increased signal acquired for stars that are observed 13 times as long as most stars in the TESS fields. That permits the detection of smaller planets through increased SNR. However, it does not account for the additional scientific benefit of being able to observe the stars for a longer time baseline, and therefore the ability to discover long-period transiting planets, some of which may be in the habitable zone. It also does not account for the longer dwell time that could potentially permit the detection of planets in configurations that a shorter dwell time would allow, such as planets in circumbinary systems (through transit detection or eclipse timing variations) or planets orbiting variable stars in which the stellar activity can be monitored and subtracted off due to the longer monitoring time. It is the case that technical considerations may create some limitations to the number of 2-minute targets that can be placed in the CVZs, but those technical issues have not yet been addressed in detail within the TESS mission. *Because of the large fraction of high priority CTL targets in the CVZs, any plot or evaluation of the distribution of stellar properties in the CTL, especially when limited to likely TESS targets (the top 400,000 stars in the CTL), must account for this effect.*

The current prioritization scheme can therefore be qualitatively summarized as prioritizing small and bright stars, with boosts for stars in the CVZs, and penalties for stars near the galactic plane or those with significant flux contamination. In the current scheme, The top $\sim 400,000$ targets are those with priorities greater than 0.047, and the top $\sim 200,000$ targets are those with priorities greater than 0.062.

4. Summary of stellar properties, known limitations, and future work

4.1. Representative properties of stars in the TIC

Table 5 summarizes the numbers of stars in the TIC and CTL for various representative subsets.

Quantity	Number of Stars	Sub-population	Number of Stars
T magnitude	471,012,798	$T < 10$	926,465
T_{eff}	20,536,040	$T_{\text{eff}} < 4500$ K	1,238,339
Radius	20,552,534	$R < 0.5 R_{\odot}$	779,989
Mass	20,552,534	$M < 0.5 M_{\odot}$	779,037
Spectroscopic T_{eff} and/or $\log g$	1,515,694		
Proper motion	111,183,767	$\mu > 50$ mas yr $^{-1}$	4,431,502
Parallax	2,046,607		

Table 5:: Summary of basic stellar properties in the TIC and CTL.

4.2. Structure within the TIC and CTL

Because of the manner in which the TIC and CTL are assembled—where identification of the most promising targets takes priority over catalog completeness or statistical uniformity—there are structures to be found within many of its observed and calculated parameters. Here we briefly identify some of the known structures for some of the most important catalog parameters, and attempt to explain their origin.

4.2.1. Interplay of priority, flux contamination, and stellar radius

The accumulated decisions that we have made to assemble comprehensive information about potential TESS targets but to ruthlessly select for small planet detection has led to a CTL that has a great deal of heterogeneity and in some places discontinuity. A good example of that is shown in Figure 14. Here we plot the priority of CTL stars versus stellar radius, portrayed in a heatmap with color indicating average contamination ratio in each 2-dimensional bin.

In the top panel of Fig. 14, the highest priority targets typically have small radii, and relatively low contamination ratios. A notable feature is the absence of stars between about 1.1 and 2.4 R_{\odot} with low prioritization values. That feature is due to the elimination of relatively faint stars with high temperatures ($T > 12$ and $T_{\text{eff}} > 5500$ K), as described in § 3.1. Because the only stars remaining in that temperature range (which is effectively a range in stellar radius since all stars here are treated as dwarfs) are relatively bright, with $T < 12$, they have a higher priority at a given contamination ratio than stars just below the T_{eff} cut.

The bottom panel of Fig. 14 shows what happens when we add back in the stars in the CVZs and near the galactic plane. Since those stars had their priorities boosted and de-boosted, respectively, they show up above and below the existing population, with similar patterns.

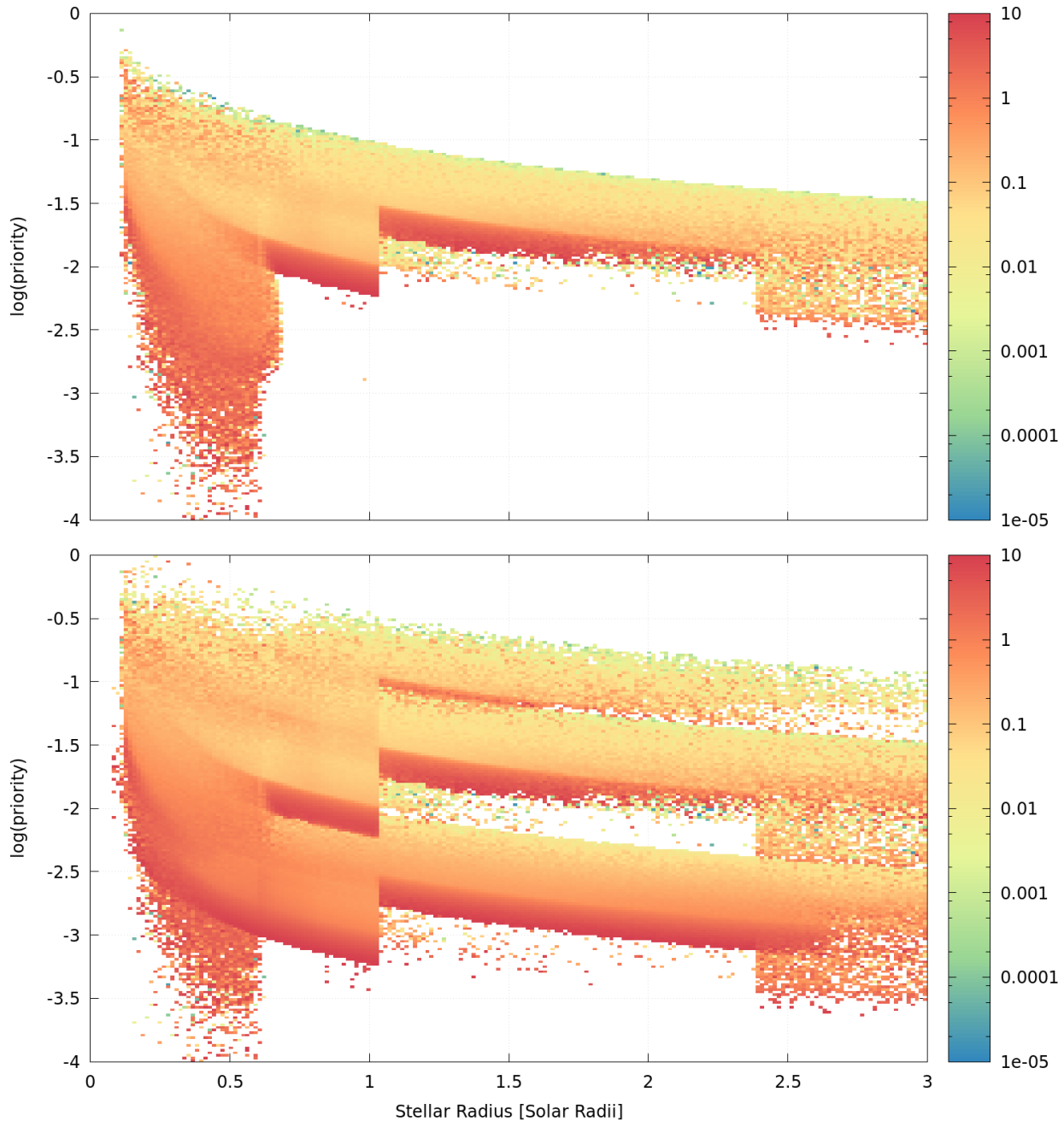


Fig. 14.— Heatmaps of CTL priority as a function of stellar radius. In general, the smaller the radius the higher the priority, as is to be expected. *Top*: The color coding as a function of flux contamination ratio shows that highly contaminated stars tend to have lower priority. In this panel the galactic plane and CVZs are excluded. *Bottom*: Same as above, only including the galactic plane and the CVZs. The structure of the data in both panels is described in the text.

4.2.2. Bimodal distribution of stellar T_{eff} : “Missing” K dwarfs

The distribution of stellar temperatures in the CTL shows a bimodal distribution, with a “gap” among the K dwarfs (Figure 15). This may seem surprising, as surely K dwarfs are more abundant than G dwarfs.

However, we have verified using a TRILEGAL population synthesis simulation (Figure 16) that this is in fact an expected consequence of the fact that we prioritize according to a combination of stellar brightness (brighter stars receive higher priority) and stellar radius (smaller stars receive higher priority). The G dwarfs benefit from the boost according to brightness, whereas M dwarfs benefit from the boost according to size, where we have intentionally inserted a specially curated sample of (generally faint) M dwarfs into the CTL. K dwarfs suffer in priority due to being relatively faint but not as small as M dwarfs.

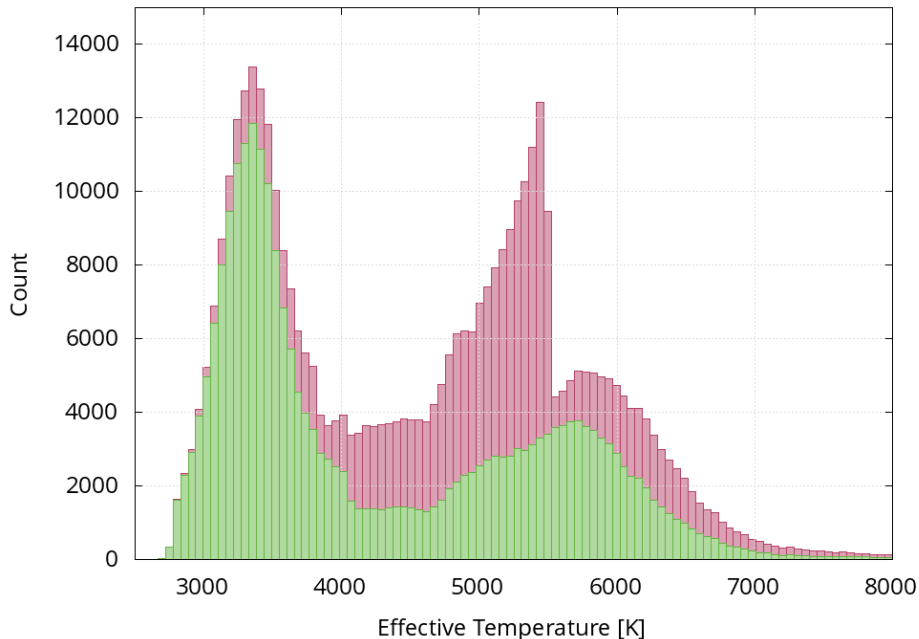


Fig. 15.— Distribution of the top $\sim 400,000$ stars in the CTL according to T_{eff} , within the CVZs (green) and outside the CVZs (red). Note the dearth of stars with T_{eff} corresponding to K dwarfs.

It is also especially worth noting the nature of the T_{eff} distribution in Figure 15 between the stars in the CVZ and elsewhere. The area outside the CVZs includes a set of early-type stars in the F and G regime, a smaller population of K dwarfs, and a large number of cool dwarfs in the late-K and early - to mid-M ranges. However, in the CVZs, there are simply not many late-type stars above the TESS detection limits, so the priority boost in those areas results in larger numbers of relatively fainter G stars. The sharp cutoff at 5500 K is an artifact with no scientific basis, and will be revisited in future versions of the TIC.

4.2.3. Effective temperature

As described in Section 2.2.2, stars with valid V and K_S magnitudes from 2MASS should have a temperature calculated from the $V - K_S$ color. While the final reported T_{eff} follows the preference order of (1) Cool Dwarf list, (2) spectroscopic T_{eff} , (3) dereddened T_{eff} , and (4) non-dereddened T_{eff} , we expect T_{eff} to generally follow the trend of our initial $V - K_S$ relation. Indeed, Figure 17 shows general agreement between the $V - K_S$ color and the “best” selected T_{eff} using the order of precedence above.

However, as also shown in Figure 17, there is a small grouping of stars with $V - K_S < -0.1$ with a much cooler T_{eff} than expected from our $V - K_S$ relation. While the V and K_S magnitudes appeared valid in their respective catalogs, their color was too blue and therefore fell outside the validity ranges of our relation. In this case these stars defaulted to the $J - K_S$ vs. T_{eff} relation. Given that their $V - K_S$ color is so blue and yet their T_{eff} is cool, this suggests either V or K_S are incorrect, due either to a mismatch or a problem with

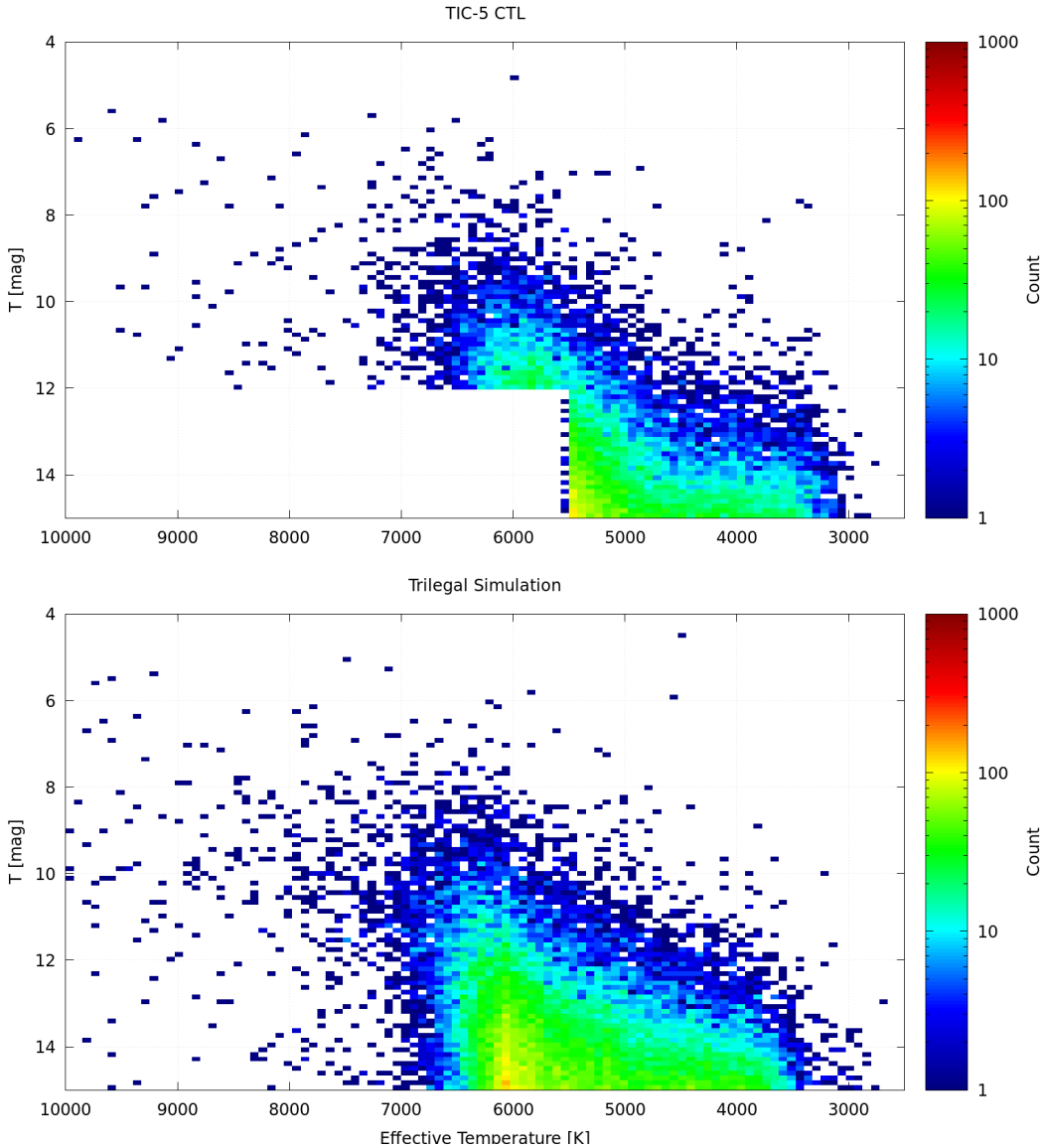


Fig. 16.— Heatmap of star counts in the CTL according to the T magnitude and T_{eff} , for real stars in the CTL (top) and for a comparable simulated population of stars from the TRILEGAL population synthesis model (bottom). The chunk of stars missing with $T > 12$ and $T_{\text{eff}} > 5500$ were removed as described in Sec. 3.1.

the original photometry. At present we do not have a mechanism to flag such cases—the quality flags from the original photometric catalogs not otherwise suggesting problems—and so we simply caution that such cases do occasionally make their way into the TIC despite our best efforts.

4.2.4. Stellar radius and mass

Figure 18 shows the calculated mass and radius for the top ~ 2.5 million stars in the CTL. While the majority of CTL stars had their radii and masses calculated from the unified spline relations described above, there are a number of objects that had their parameters calculated from spectroscopy, from parallaxes, taken

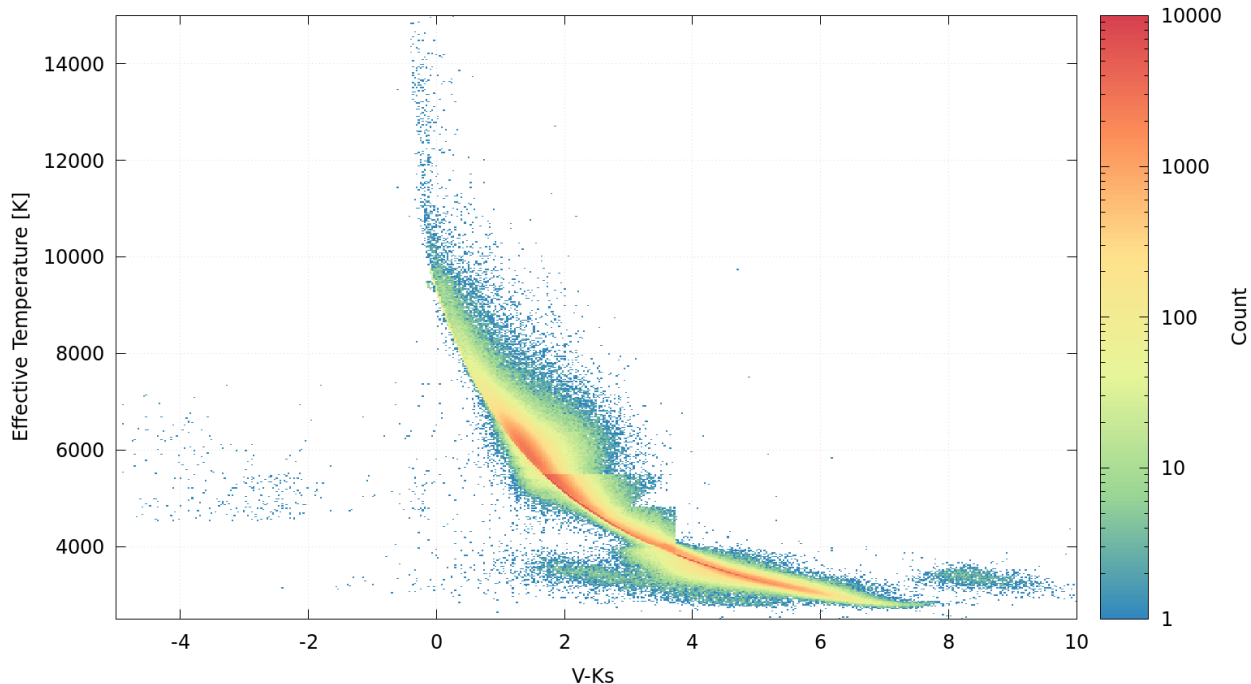


Fig. 17.— Heatmap of T_{eff} (selected as described in Sec. 4.2.3) and each star’s $V - K_S$ color for the top ~ 2.5 million high priority objects in the TIC. The points follow a basic trend but there is a “cloud” of objects for which $V - K_S < 0.1$. This feature is likely due to stars with poor V magnitudes not flagged in their respective photometric catalogs. In this case T_{eff} was calculated from $J - K_S$.

from the independent Cool Dwarf list, or a combination of these methods. Therefore Fig. 18 shows a large number of stars with masses and radii from the spline relation but also shows a cloud of points around the relation. While there is a significant spread of radii and masses for a particular T_{eff} , it is encouraging that in general the distribution of values is more or less centered on the ridge coming from our spline relation. Thus, a TIC/CTL user should expect to find stars with similar T_{eff} but differing radii or masses.

4.2.5. Proper motions

As described in Section 2.2.3, the TIC gathers proper motion information from five sources: the *Tycho-Gaia* Astrometric Solution, SUPERBLINK, *Tycho-2*, *Hipparcos*, and UCAC4. The TIC’s proper motion information is primarily used in the calculation of RPM_J values that are in turn used to provide an informed estimate of whether a star could be a dwarf or a giant (see Section 2.2.3).

While these catalogs collectively provide over 115 million proper motion measurements, UCAC4 is the source for the vast majority - more than 100 million of them. Thus, the CTL inherits many of the survey coverage features found in UCAC4. Particularly noticeable is the dearth of high priority objects with proper motion measurements below a declination of about -35° , as shown in Figure 19 (Zacharias et al. 2013). Future versions of the TIC—especially after the *Gaia* DR2 release—will have improved proper motion coverage which will help to alleviate some of these striking features in the CTL¹⁰.

¹⁰While we plan to incorporate the HSOY (Altmann et al. 2017) catalog prior to the release of *Gaia* DR2, because HSOY is based on the PPMXL catalog, like UCAC4, we expect it may have similar coverage features.

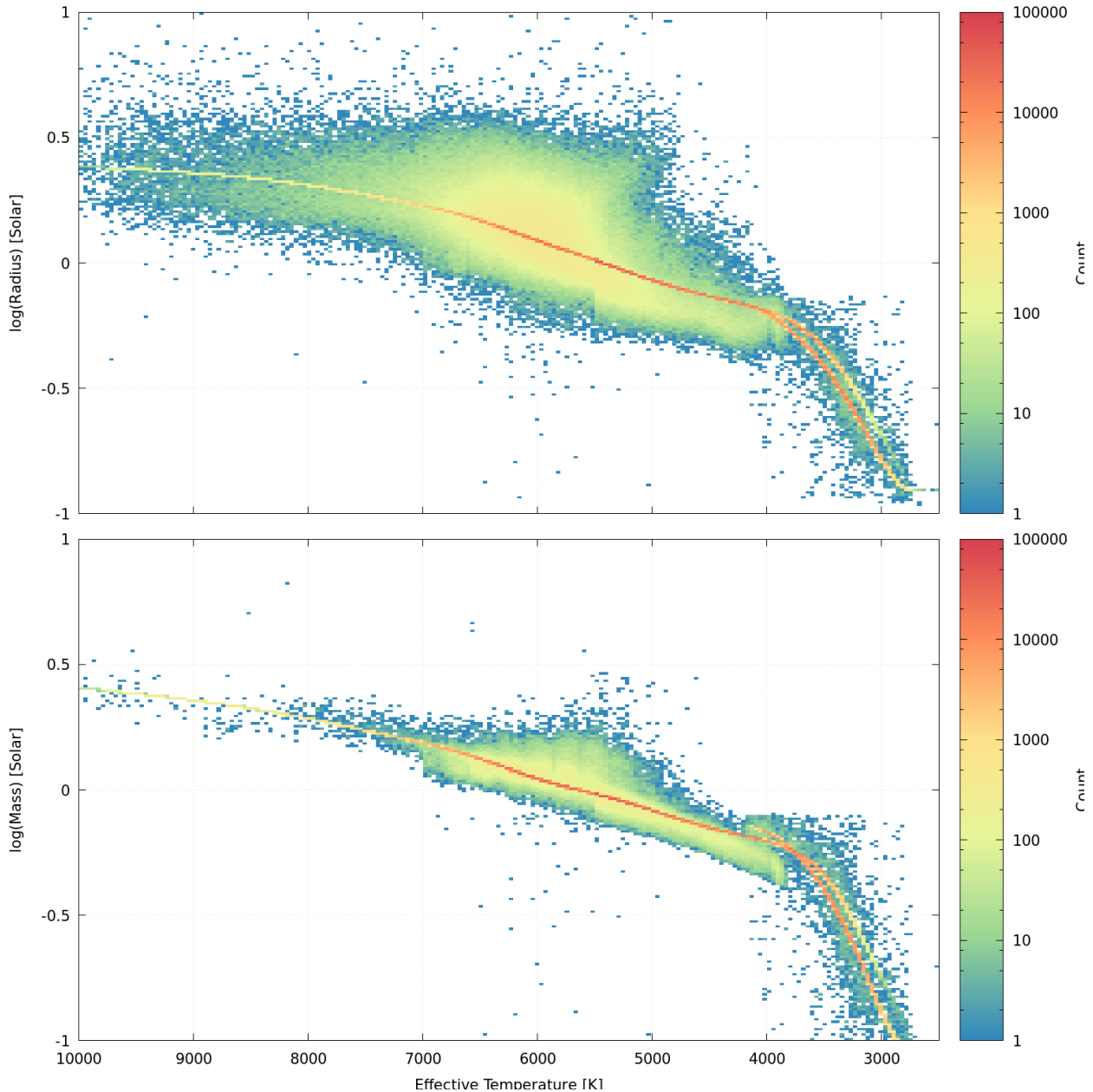


Fig. 18.— Heatmaps of the calculated radius (*top*) and mass (*bottom*) for the top ~ 2.26 million stars in the CTL. The second stellar loci for values with $T_{\text{eff}} < 4000$ K, comes from the Cool Dwarf list. The over-density of points (stellar loci) in both figures comes from the unified spline relations. While the “cloud” of points in the radius plot is due to a combination of radii from the Cool Dwarf list, the use of parallaxes, and the spectroscopic relation of Torres et al. (2010). The distribution of points in the mass plot results from a combination of Cool Dwarf list values and values from the spectroscopic relation.

4.2.6. Sky distribution of top priority objects

One of the primary purposes of the TIC and CTL is to provide a list of the top 200,000 to 400,000 targets to be observed in the 2-min cadence. If we investigate the distribution of these targets in the celestial sphere significant features begin to arise as shown in Figure 19.

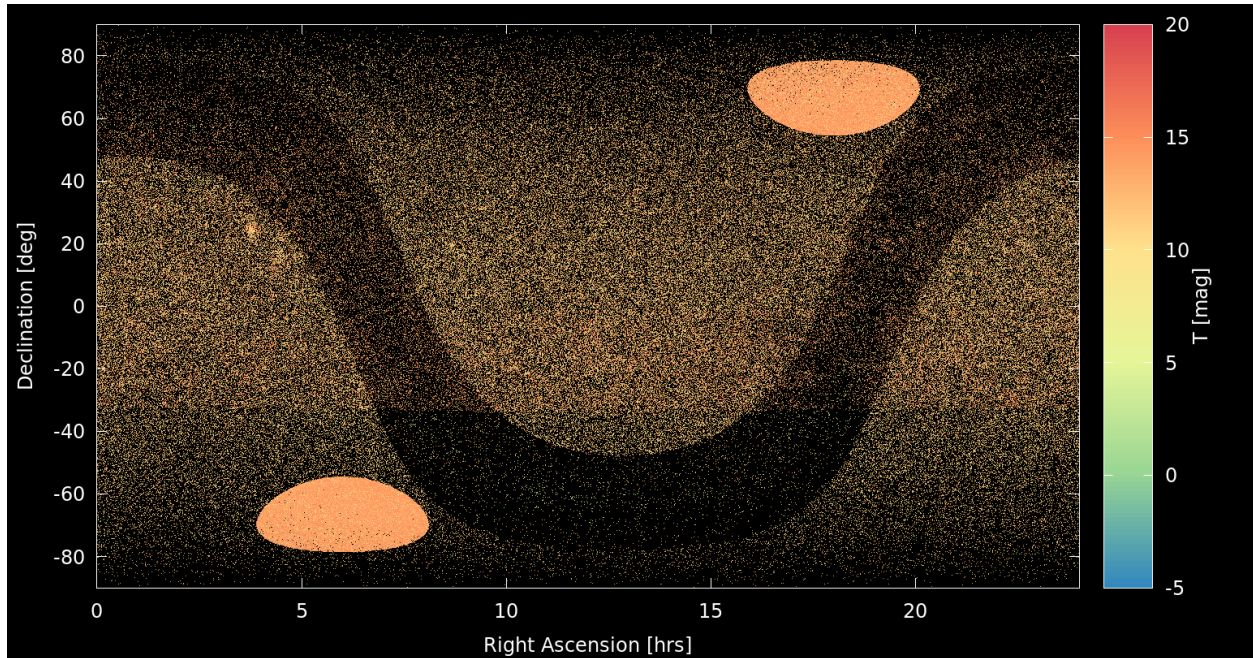


Fig. 19.— The distribution of top CTL targets in right ascension and declination, colored by T magnitude. Clear patterns arise due to de-boosting in the Galactic Plane ($|b| < 15^\circ$), the special boosting within the ecliptic poles ($|\beta| > 78^\circ$), and the coverage of the proper motion catalogs (the lines near -35°).

The most notable feature is the dearth of stars in the Galactic Plane. Because confusion is large in the plane, we de-boosted stars that do not have spectroscopic T_{eff} or that are not included in any special catalog. Secondly, there is a clear demarcation at about -35° in declination. This is due to the proper motions of the majority of TIC stars coming from the UCAC4 survey, which is based on the PPMXL catalog, and as described above this catalog is deficient at these southern declinations. Finally, the two elliptical regions at the northern and southern ecliptic poles ($|\beta| > 78^\circ$) are the CVZs. Because the priority boost given to stars in those regions, they are quite overdense compare too the rest of the sky.

4.3. Known limitations and plans for improvement

4.3.1. Stellar Activity and RV Followup

So far the prioritization of candidate transit targets has been based on estimates of the detectability of transits produced by small planets, and assumptions on the geometric parameters (e.g., stellar radius) and measurement noise (e.g., stellar brightness and flux contamination by neighbors). However, in principle it should be possible to also prioritize based on the likely photometric and/or radial-velocity quiescence of the star. Photometric noise from, e.g., magnetic activity could complicate the detection of small transit signals, whereas radial-velocity noise (e.g., ‘jitter’) could complicate the confirmation of planets and the measurement of stellar masses. With regards to photometric noise, there are a number of long-term photometric monitoring campaigns of bright stars across the sky that could be used to obtain a measure (or at least an upper limit) on the amplitude of photometric variability. Surveys that could be utilized for this purpose include SuperWASP and KELT, as well as ASAS (Pepper et al. 2007, 2012; Smith & WASP Consortium 2014; Pojmanski 1997).

With regards to radial-velocity jitter, most RV surveys cover relatively few stars. However, in principle it would be possible to use a proxy such as stellar rotation, either spectroscopic ($v \sin i$) or photometric

(rotation period). For example, Vanderburg et al. (2016) gives empirical relations linking radial velocity jitter to stellar rotation period as a function of stellar T_{eff} .

We are in the process of determining measures of stellar rotation period and variability amplitudes from the entire set of KELT-North and KELT-South light curves. Because the KELT and TESS pixel scale, field of view, and depth are comparable (see Pepper et al. 2007, 2012), we anticipate that the KELT photometric variability measures may prove useful in further winnowing the CTL of stars that might otherwise be too photometrically or Doppler noisy.

4.3.2. *Binarity*

It is known that most stars are in gravitationally bound pairs or stellar systems of higher multiplicity (e.g., Duchêne & Kraus 2013). All-sky or wide-field catalogs of stars are often able to separately identify the individual stellar components of especially wide binary pairs, in which both stars are bright enough for detection, but generally are not able to resolve the components below a certain angular separation, or detect fainter companions. Furthermore, even when all components in a multiple system are individually identified, it is typically not possible to reliably match the bound stars without good proper motion or other dynamical information. Therefore, we expect that a large fraction of the stars in the TIC either represent blended, unresolved multiple stars, or members of multiple systems with the other components not identified.

Binarity and higher multiplicity affects the reliability and integrity of the TIC, since an unresolved companion will cause the photometric measurements of a star to be incorrect, along with any derived stellar properties such as T_{eff} , mass, and radius.

Furthermore, the presence of stellar companions specifically affects the suitability of a star as a TESS mission target, even if the stellar properties of the target star are correctly described. That can happen by introducing signals that complicate or confuse the transit search, or by creating conditions that would not permit the presence of any planet that TESS is capable of detecting. In the first category, if a stellar companion is in orbit about the target with a period shorter than the TESS dwell time on the target and happens to be eclipsing, the system can mimic the photometric signal of a transiting planet. That can happen if the companion is in a grazing orbit, or if the companion is a small enough star to create an eclipse comparable to the transit of a planet. Or, if there is a planet transiting the target on a stable interior orbit, the photometric signal of the eclipsing companion can interfere with the ability to detect the transit signal. Also, the presence of a luminous stellar companion unresolved from the target will dilute the photometric transit signal.

In the second category, the presence of a stellar companion indicates that there could not exist a planet in an orbit around the target star that TESS could detect, meaning that the target could potentially be excluded from the 2-min target list if the presence of the companion were known. Generally, the presence of a stellar companion in an orbit of a given size will dynamically exclude planetary companions in a range of orbits (e.g., Kraus et al. 2016). Also, a stellar companion with a short orbital period may indicate the absence of any circumbinary planets.

For those reasons, it would be advantageous to know about the existence of all stellar multiplicity for each potential target star. That information is generally not available but will be critical for establishing the correct planetary radii (Ciardi et al. 2015). We are endeavoring to obtain whatever information is available, through lists of known multiple systems from stellar spectroscopy that can identify single- and double-lined spectroscopic binaries, photometric surveys that can identify eclipsing systems, proper motion catalogs that can identify co-moving companions, and eventually time-series astrometric catalogs to identify astrometric binaries. However, we expect all such efforts to be quite incomplete due to various observational biases.

4.3.3. *Gaia DR2*

It had been hoped from the start of planning for TESS target selection that the highly anticipated *Gaia* DR2 parallaxes might become available prior to TESS launch. Unfortunately, at this writing, it appears unlikely that this will be the case. Nonetheless, we are planning to incorporate the *Gaia* DR2 parallaxes when they do become available. For example, even if these parallaxes do not become available until several months after launch, they could still be used to refine the target selection procedures for the second ecliptic hemisphere to be observed in Year 2 of the mission.

There is at least one specific area in which the incorporation of the *Gaia* DR2 parallaxes could dramatically enhance target selection: elimination of subgiant contaminants. As discussed by Bastien et al. (2014) in the context of the bright *Kepler* targets, roughly half of the putative dwarf stars are in fact modestly evolved subgiants, whose slightly lower $\log g$ values are too subtle for discernment by photometric and even some spectroscopic methods. Moreover, as discussed above (Section 2.2.3), the reduced-proper-motion method that we employ to screen out red giants is also ineffective at removing most subgiants. As laid out in Section 3.2.2, with an accurate parallax for most if not all TESS targets, we can accurately determine the stellar radius and thereby screen out subgiants with high fidelity. In the meantime, a large proportion of subgiant contaminants are to be expected among the putative dwarf stars in the CTL.

Finally, with *Gaia* magnitudes available for virtually all stars in the TIC, it should be possible in principle to re-determine accurate T magnitudes for all TIC stars.

4.3.4. *Special plans for CVZs and other prioritization considerations*

Section 3.3 discussed the current prioritization scheme. That algorithm provides a boost in priority for stars in the CVZs by a factor of $\sqrt{13}$ because stars in that region can be observed 13 times as long as other stars, and hence their light curves will have an increase in transit SNR for planets with short periods. However, such stars benefit in other ways. The longer observing duration permits the detection of planets in longer orbits. The orbital period parameter space also allows TESS to probe regimes where circumbinary planets may be detected. Since the TESS CVZs overlap with the planned JWST CVZs, planets detected in these regions will be more accessible for detailed atmospheric follow-up by that mission.

For those reasons, a star in the TESS CVZs presents greater potential science return than one elsewhere, and the prioritization of those stars should be increased. However, it is not yet clear how to parametrize that greater scientific potential and thence incorporate that information into the prioritization algorithm.

There are at least three other aspects of each star that can affect planet detectability, which are not yet incorporated into the CTL target prioritization scheme. They are:

1. Number of TESS observations, determined by placement in overlap regions, and which will only be known before launch for a subset of the targets.
2. Suitability for dynamical confirmation. Stars for which it will be harder to get spectroscopic (radial-velocity, RV) orbits should be given lower priority for the same size minimum detectable planets. This consideration can include intrinsic RV stability, levels of chromospheric activity, rotational velocity, or even projected rotational velocity (which can be used to tell which exoplanetary ecliptics are edge-on, assuming typical systems have low inclination).
3. There are other properties of stars that correlate with either planet frequency or planet properties, such as T_{eff} and metallicity: high metallicity yields more giant planets, and low T_{eff} may yield more small planets. It is unclear how those considerations can be incorporated into the prioritization scheme. See, e.g., Newton et al. (2016).

4.3.5. Full-frame images

In addition to the standard 2-min cadence of measurements for the primary 200,000–400,000 bright transiting planet candidates, TESS will provide full-frame images (FFIs) with a cadence of 30 min. These FFIs can in principle be used to also identify planetary transits, and thus it may be beneficial to consider which types of transit hosts can be effectively studied at 30-min cadence so as to reserve as many 2-min slots for those types of systems that most require the higher cadence. Here we consider two types of situations where such a consideration could lead to further optimization of the CTL.

Transits of M dwarfs and White Dwarfs by Earth-sized planets

There are systems where there could be transits with durations less than an hour or so, i.e., short enough that the SNR for detection starts to be significantly compromised if they are only observed with a 30-min cadence. It is fairly likely that transits could be non-equatorial and have durations as short as 30–50% that of an equatorial transit. Especially considering the possibilities of non-equatorial transits, and that orbits could have semimajor axes as tight as $\sim 3 R_*$, some systems could even have transits that are much shorter than 30 minutes.

One approach would be to propose that the highest priority for inclusion in the CTL be those systems where it is reasonably possible that there could be transits shorter than one hour. This would include all white dwarfs and all low-mass main-sequence stars. The faint end of the magnitude range would tentatively be $T \sim 14$, and the upper mass cutoff would be $\sim 0.5 M_\odot$ for main-sequence stars. These notional parameter cutoffs are justified as follows.

We have performed crude calculations regarding the transits of $0.1\text{--}1.0 M_\odot$ main-sequence stars by small planets, i.e., planets with radii that are much smaller than those of their host stars. For these stars we take the mass-radius relation to be $M_*/M_\odot \approx R_*/R_\odot$. The equatorial transit duration is then: $t_{\text{eq-dur}} = P_{\text{orb}} 2R_*/(2\pi a)$, where P_{orb} is the orbital period, R_* is the radius of the host star, and a is the semimajor axis of the planetary orbit. The close-in orbits are the ones that might make very short transits. We take the “relatively likely” extreme close-in case to be $a = 3R_*$. Then $t_{\text{eq-dur}} = P_{\text{orb}}/10$, roughly speaking. Using Kepler’s third law with $a = 3R_*$ and the above mass-radius relation, we obtain $P_{\text{orb}} \approx 0.6(R_*/R_\odot)^{1/2}$ days. For a star with $M = 0.2 M_\odot$ this gives $P_{\text{orb}} = 6.4$ hrs. Indeed, at least one planet has been found around a low-mass star with an orbital period in the range of 4–5 hrs.

Continuing, we obtain $t_{\text{eq-dur}} \approx P_{\text{orb}}/10 = 0.06(R_*/R_\odot)^{1/2}$ days = $1.4(R_*/R_\odot)^{1/2}$ hrs. This gives a 1-hr transit duration for a planet orbiting a star with $M = 0.5 M_\odot$ at $3R_*$. It gives a duration of ~ 0.5 hr for a planet orbiting a $0.1 M_\odot$ star at $3R_*$. These are the durations of equatorial transits; non-equatorial transits will be a bit shorter. A transit impact parameter of 0.86, which is admittedly extreme, gives a transit that is half the duration of an equatorial transit.

A star with $M = 0.1 M_\odot$ may be very unusual in TESS observations. Stars with $M \sim 0.2\text{--}0.3 M_\odot$ should be more frequent targets. This suggests that $0.5 M_\odot$ may serve as a reasonable upper mass limit for this category. There should also be a faint magnitude limit based on detectability of these short periods in an FFT or Box Least Squares (BLS; Kovács et al. 2002) search of a 27-day or longer observation. We have not yet attempted that calculation, which would depend on the planet radius as well as the other assumptions made above. We have also neglected the planet radius in computing the transit duration. Large planets on such orbits would be detectable even around fairly faint stars, but the transits would be a bit longer than calculated. Small planets would of course be harder to detect.

In principle, stellar mass and radius estimates are also needed. However, in practice, one might assume all targets are main-sequence (except for white dwarfs) and the above mass-radius relation may be sufficient.

Transits of hot subdwarfs by Earth-sized planets

Hot subdwarfs represent another potentially interesting class of transiting planet host star that, because of the small stellar radius, may require the 2-min cadence observations in at least a subset of cases. The transit duration of a subdwarf star by a planet with a radius of $1 R_{\oplus}$ is shown in Figure 20 as a function of orbital period and the $\log g$ of the host star.

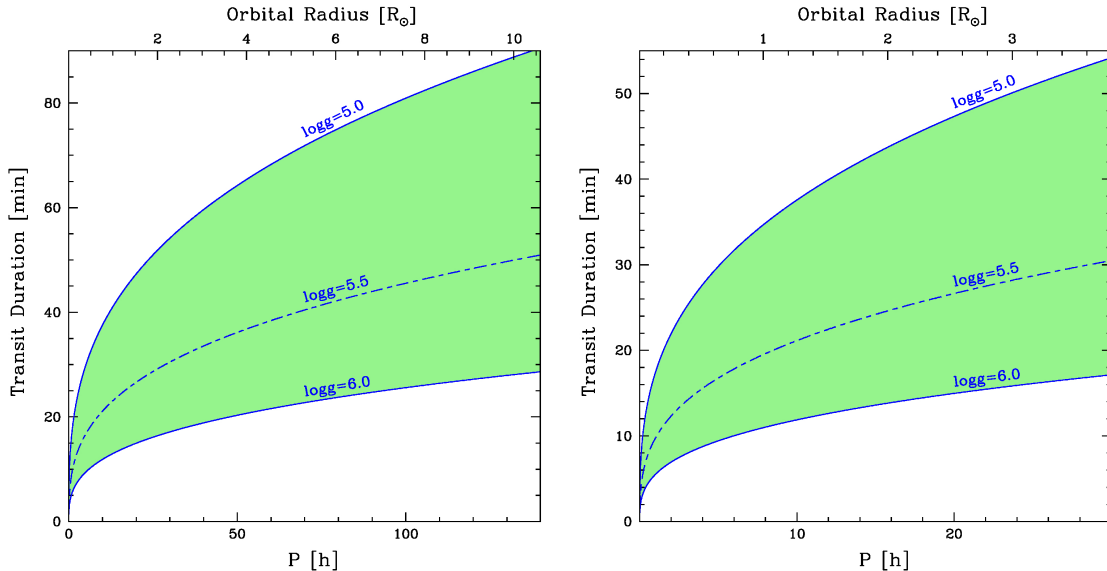


Fig. 20.— (Left) Duration of the transit of a hot subdwarf by a planet with a radius of $1 R_{\oplus}$, as a function of orbital period and $\log g$ of the host star. (Right) Detail at short orbital periods.

4.3.6. Effects of reddening on the T magnitude

In a future version of the TIC, we will need to account for the effects of reddening and extinction on T . The color relations we are using are derived from model atmospheres that assume the fluxes are not affected by extinction, which is not true in practice. We plan to overcome this approximation by correcting our $V + JHK_S$ magnitudes for extinction and then, using the de-reddened fluxes, we will derive an extinction-free TESS magnitude with the previously described relations and coefficients. We will then apply the appropriate extinction for the TESS band to recover an “observed” TESS magnitude. Using the Cardelli et al. (1989) extinction law with a weighted mean wavelength for the passband and ignoring the spectrum of the star, we estimate $A_T = 0.656 E(V - K_S)$, $A_J = 0.325 E(V - K_S)$, and $A_G = 0.901 E(V - K_S)$, where G is the *Gaia* magnitude we expect to incorporate into a future version of the TIC. The conversion from $E(V - K_S)$ to $E(B - V)$ can be made with $E(B - V) = 0.372 E(V - K_S)$, and similarly $E(G - J) = 0.576 E(V - K_S)$. For stars that do not have a reliable V magnitude no extinction correction will be computed.

Figure 21 shows the expected differences between TESS magnitudes calculated without proper consideration of extinction and those with extinction accounted for, for extinction levels of $A_V = 1$ and $A_V = 3$. For most stars in the TIC experiencing modest extinction, the impact of not properly modeling the effect amounts to a systematic error of ~ 0.1 mag for the coolest stars. However, for areas of high extinction such as in the Galactic plane the effect can be as large as several tenths of a magnitude for $T_{\text{eff}} \lesssim 4000$ K.

It is a pleasure to thank the members of the TESS Target Selection Working Group for input into the

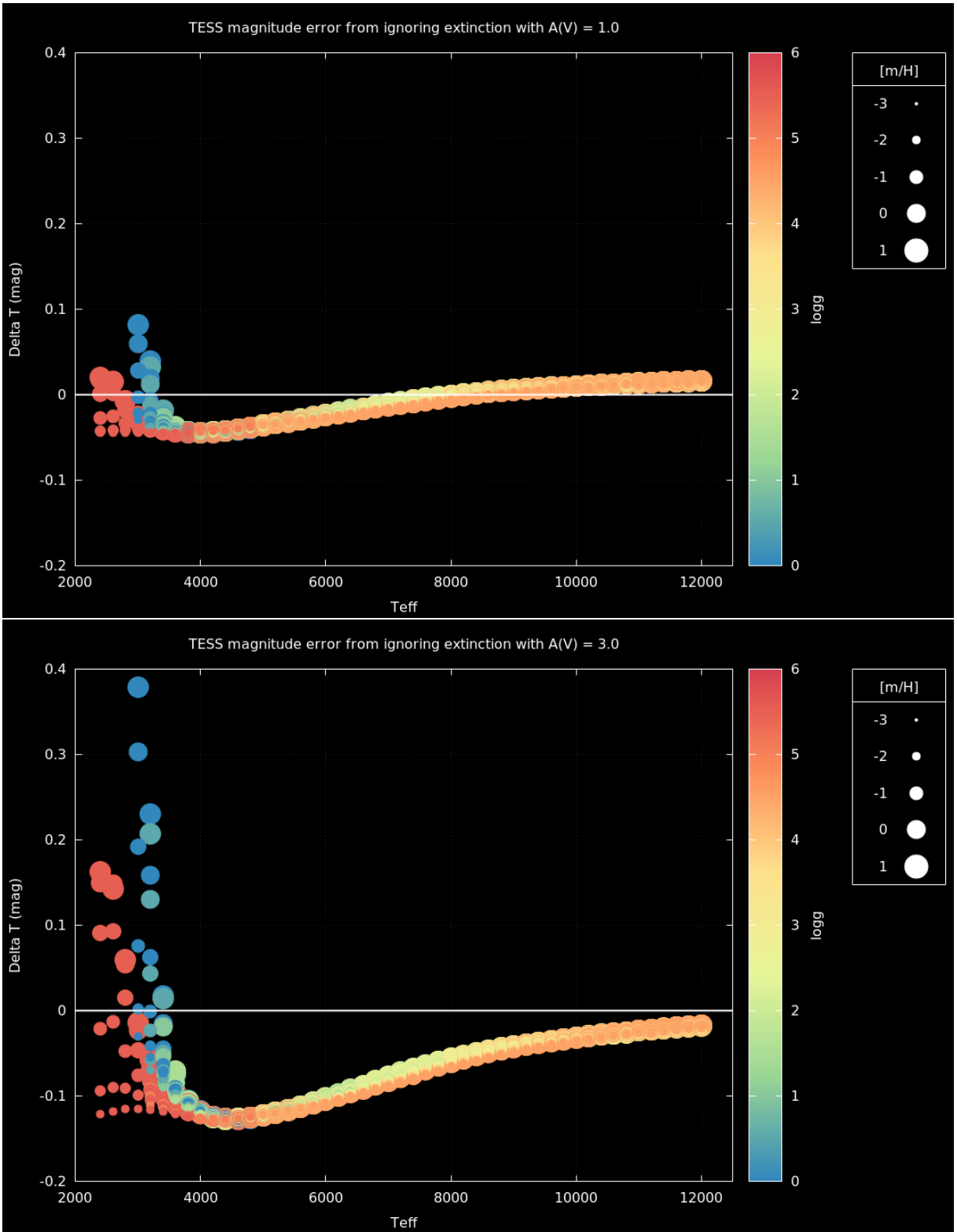


Fig. 21.— (Top) Error in the calculated TESS magnitude if extinction is ignored and the true extinction is $A_V = 1.0$. (Bottom) Same as above for $A_V = 3.0$.

development of the procedures described here, including especially contribution of the special target lists discussed above. This work has been partially supported by the NASA TESS mission through a subaward to Vanderbilt University.

A. TIC-5 Release Notes

TESS Input Catalog Version 5 (TIC-5) Release Notes 2017-05-23

This delivery contains the fifth version of the TESS Input Catalog (TIC) produced entirely by the Target Selection Working Group (TSWG), and was delivered to the TESS Science Office (TSO) on 2017 May 23.

The delivery has a number of minor issues (see below) which have not been fixed in this version due to time constraints during preparation. Specific details of the method of production and the contents of this TIC are described in detail in the full TIC Documentation on arXiv.org <https://arxiv.org/abs/XXXX.XXXX> and are not repeated here.

The format used is the same as TIC-4, in that the specific columns and their format are the same, but there have been significant changes compared to TIC deliveries prior to TIC-5. TIC IDs have not been changed and all future deliveries of the TIC will use the same IDs for specific objects, and new objects added will receive new IDs.

Changes compared to TIC-4

This delivery contains major changes in computed quantities compared to TIC-4. It should be noted the methods used to estimate a variety of the stellar parameters are still under active development and can be affected by poor catalog photometry when there is no acceptable alternative photometry for a given star. The major changes compared to previous versions are:

1. An internal database error in the reduced proper motion selection in TIC-4 was corrected. Originally, this error resulted in ~ 11 million likely dwarfs being excluded from the TIC-4 CTL and ~ 600 K stars which are likely giants being included in the CTL. The error has been corrected, the contaminants removed and the possible dwarfs included in the new CTL selection (see 5 & 6 below).
2. We now define a 0.05 mag area to the left of $V - Ks \leq 2.2241$ above the polynomial fit to the data from Bessell & Brett (1988; see Figure 10 in the documentation). Stars within this area are assumed to have zero reddening and have been flagged as “dered0”.
3. We now select a maximum $E(B - V)$ value of 1.5 rather than 15.
4. The priority calculation has been updated to properly represent the dimensionality involved with combining TESS’s expected photometric precision and expected contamination ratio for a given source. The contamination ratio and photometric error are now combined as $\sqrt{\epsilon + 1}\sigma \times 10^{-6}$, where ϵ is the contamination ratio and σ is the expected photometric precision in ppm.
5. In addition to requiring CTL stars to be RPM_J dwarfs and have $T < 15$ (unless in a special target list), the CTL now excludes stars where $T > 12$ and $T_{\text{eff}} > 5500$ K.
6. Any star with $J - H > 0.75$ is now excluded from the CTL (even if it is identified as a reduced proper motion dwarf) unless it is included in the cool dwarf list or has a spectroscopic T_{eff} .
7. We have implemented a variety of internal consistency checks to ensure parameters such as mass, radius, $\log g$, etc., are all consistent with one another assuming they are from different sources. See Appendix D of the documentation for more details.

8. Stars within 15 deg of the Galactic Plane ($|b| < 15^\circ$) have their priorities de-boosted by a factor of 0.1.
9. Minor fixes and exclusions of stars left in the CTL from legacy versions of the cool dwarf list.
10. The contamination ratio no longer uses the galaxies as possible contaminants. The galaxy distribution is expected to be homogeneous across the sky and eliminating the galactic contamination relieves much of the structure present in the priority distribution of top targets.
11. The CTL now incorporates a "Bright Star" special target list. This includes all stars in the TIC with $T < 6$. Contamination ratios were calculated for this target list and priority values were set to be 1. These stars, in most cases, do not have all stellar parameters, such as mass and radii, calculated.

Notes on the individual columns:

No.	Name	Notes
7	SDSS	The values given are the 64-bit "objID" values, not the IAU-format "SDSS J" identifiers.
9	GAIA	In TIC-5 we only include Gaia object IDs for the Gaia-TGAS subsample.
10	APASS	APASS stars do not have an identifier, only coordinates. We use the primary key of an internal TESS version of the APASS database table as a proxy identifier.
17	pmRA	The RA proper motions, in order of preference, are (1) Gaia-TGAS, (2) Superblink, (3) Tycho-2, (4) Hipparcos, and (5) UCAC4. If a star did not have a proper motion in these catalogs, it is not provided.
19	pmDec	The Dec proper motions, in order of preference, are (1) Gaia-TGAS, (2) Superblink, (3) Tycho-2, (4) Hipparcos, and (5) UCAC4. If a star did not have a proper motion in these catalogs it is not provided.
22	plx	The parallax values, in order of preference are (1) Gaia-TGAS, and (2) Hipparcos. Some values are negative because of the way the parallaxes were measured in TGAS and Hipparcos.
29	Bmag	Johnson B magnitude. When a Johnson B magnitude was not found in one of the optical catalogs, the TIC reports a Johnson B derived from the USNO-A2.0 magnitude given in the 2MASS catalog.
59	Gmag	Gaia magnitudes are included in TIC-5 only for the TGAS subsample.
61	Tmag	This column is never NULL. The Tmag values are typically based on relations that depend on J and V-Ks or J-Ks (see column 63 for method flag). TESS magnitudes for objects for which only poor catalog photometry was available were computed simply as offsets from a reference magnitude (see Documentation Section 2.2.2).
63	TESSflag	These flags denote which relation or catalog provides the TIC TESS magnitude: from_apass_i: Cool Dwarf provided magnitude. from_sdss_i: Cool Dwarf provided magnitude. hipvmag: Tmag calculated from Cool Dwarf list cdwarf: Tmag calculated from Cool Dwarf list hoffset: Tmag calculated from 2MASS H + offset.

joffset: Tmag calculated from 2MASS J + offset.
koffset: Tmag calculated from 2MASS Ks + offset.
lepine: Tmag calculated using the V magnitude from the Lepine catalog
bpjk: Relation using 2MASS JKs and photographic B.
jhk: Relation using 2MASS JHKs.
vjk: Relation using 2MASS JKs and Johnson V.
voffset: Tmag calculated from V + offset.
wmean_vk_jhk: Cool Dwarf provided magnitude.
tmvk: Relation using 2MASS calculated V and Ks.
jh: Relation using 2MASS JH.
sdss: Relation for extended objects using Sloan g and i.

See TIC-5 Documentation Section 2.2.1 for details of each method. While most of these relations (which are used for most Tmag values) are only appropriate for dwarf stars, some are applicable to giants. Extended objects were treated as if they were dwarfs. In general the dwarf relations are strictly valid between specific color ranges and tend to be less accurate for very blue stars ($J-Ks < -0.1$) or very red stars ($J-Ks > 1$).

64 SPFlag These flags denote the origin of stellar characteristics:
cdwarf: mass and radius provided by the Cool Dwarf list
plx: characteristics computed from measured parallax
spect: characteristics computed using the spectroscopic Torres relations
allen: characteristics computed from Teff using modified relations from Allen's
Astrophysical Quantities
normal: same as allen, naming artifact to be removed in future releases

Stellar parameters provided in the specialized Cool Dwarf catalog always override photometrically determined quantities. If a given star has spectroscopic parameters provided in one of the catalogs below, these values also take precedence over photometrically derived parameters but do not override quantities from the Cool Dwarf list. The catalogs used in the TIC, and their order of preference, are: (1) SPOCS, (2) PASTEL, (3) Gaia-ESO, (4) GALAH, (5) APOGEE DR-1, (6) LAMOST DR-1, (7) RAVE DR-4, and (8) Geneva-Copenhagen. When more than one value for a given star is present in a given spectroscopic catalog, all values were combined using a weighted mean.

65 Teff The effective temperatures come from one of four sources, in the following order of preference: (1) the Cool Dwarf list; (2) spectroscopic catalogs (see Column 64); (3) dereddended V-Ks color; and (4) non-dereddended V-Ks color. Please note that all stars with Teff < 3840 K have been excluded from any de-reddening, on the assumption that they are nearby M dwarfs.

66 e_Teff The SPOCS and GALAH catalogs do not provide uncertainties for effective temperatures; 25K and 41K were assigned, respectively, based on the reported statistical error from those catalogs.

68 e_Logg The SPOCS and GALAH catalogs do not provide uncertainties for surface gravities; 0.028 and 0.17 dex were assigned, respectively, based on the reported statistical error from those catalogs.

70 e_M/H The SPOCS and GALAH catalogs do not provide uncertainties for metallicities; 0.10 and 0.05 dex were assigned, respectively, based on the reported statistical error from that catalog.

- 71 **Mass** If an object's mass is provided in the specialized Cool Dwarf list it is included in the TIC. Otherwise, the stellar masses were estimated using a relation based on measured masses for eclipsing binaries as well as simulations using Galactic structure models.
- 73 **Radius** The stellar radii were estimated using a variety of techniques, in the following order of preference: (1) the Cool Dwarf list; (2) spectroscopic relations from Torres et al. 2010, A&ARv, 18, 67; (3) using the Gaia parallax and bolometric corrections; and (4) a unified relation based on measured radii for eclipsing binaries as well as simulations using Galactic structure models.
- 77 **LumClass** This is a boolean dwarf flag. If this is set, LumClass = DWARF, or otherwise GIANT. SUBGIANT is not used at present. However, the DWARF flag for TIC-5 effectively means that the star is either a dwarf or a subgiant, based on reduced proper motion cuts.
- 82 **E(B-V)** Stars for which $E(B-V) > 1.5$ have their $E(B-V)$ values set to a maximum of 1.5.
- 85 **contratio** The contamination ratio is defined as the nominal flux from the contaminants divided by the flux from the source. Flux contamination is calculated for all stars identified as dwarfs that are brighter than $T_{\text{mag}}=15$, or are in special target catalogs such as the Cool Dwarf list. Contaminants are searched for within 10 TESS pixels of the target and the contaminating flux is calculated within a radius that depends on the target's T_{mag} . The PSF is modeled using a 2D-Gaussian based on preliminary PSF measurements from the SPOC.
- 88 **priority** Priority of target for observation. This is a floating-point value ranging from 0 to 1, where 1 is highest priority. The priority is based on the relative ability of TESS to detect small planetary transits, and is calculated using the radius of the star, the contamination ratio, and the total expected photometric precision. Stars within the continuous viewing zones ($|b| > \sim 78$ deg) are given a boost to their priority by a factor of $\sqrt{13}$, as they will be observed roughly 13 times longer than the majority of TESS targets. Stars within the Galactic Plane ($|b| < 15$) have been de-boosted by a factor of 0.1 since we generally have a poor understanding of their true de-reddening.

The following columns are not populated:

No. Name

83 e_EBV

86 Disposition

Known issues and pitfalls:

There are a number of minor issues that have been identified by the TSWG. We expect to address these issues in a future version of the TIC. The issues include:

1. All coordinates are for the epoch of observation (often 2MASS or SDSS). Epochs are not currently supplied.
2. Because some stars have poor quality 2MASS photometry flags (such as 'D', 'U'), offsets were applied to V , J , H , or K_S magnitudes to provide a more realistic TESS magnitude but may be different from the true value by a magnitude or more.
3. There is a clear pattern in the sky distribution of top CTL stars. This is a combination of three effects: The first is from the SuperBlink/UCAC4/Proper Motion Catalogs. The edge at about -30 deg is due to the incompleteness in these catalogs. The second effect is the priority boost to stars in the CVZ,

typically any star with an ecliptic latitude greater than 78 deg is more likely to have a high priority. The third effect is the priority de-boost to stars within 15 deg of the Galactic Plane by a factor of 0.1.

Planned Improvements in Future Versions:

There are a number of planned improvements for future versions of the TIC. At present these improvements include:

1. A refinement of the algorithm for calculating the expected photometric error on the T magnitude, to include properties such as the coordinates in order to properly account for zodiacal light.
2. All coordinates to be prepared in equinox J2000.0, and epoch 2000.0.
3. Create a more extensive list of stars with known radii and masses, so that we can test improved mass and radii relations.
4. Fully incorporate the *Gaia* catalog(s) into the calculation of the TESS magnitudes, positions, and source IDs.
5. Improve the dwarf/subgiant/giant discrimination using *Gaia* information.

B. TIC columns, formats, and minimum/maximum permitted values

In Table 6 we describe each column found in the TIC, its data type, basic column description, and the minimum and maximum allowed values. If the column is never permitted to be null (NN = ‘never null’), it is also indicated.

Column	Name	Type	Description	Min	Max	NN?
1	ID	I10	TESS Input Catalog identifier	1	10 ¹⁰	NN
2	Version	A8	Version Identifier for this entry [yyyymmdd]	–	–	–
3	HIP	I6	<i>Hipparcos</i> Identifier	–	–	–
4	TYC	A12	<i>Tycho-2</i> Identifier	–	–	–
5	UCAC	A10	UCAC4 Identifier	–	–	–
6	TWOMASS	A16	2MASS Identifier	–	–	–
7	SDSS	A20	SDSS DR9 Identifier	–	–	–
8	ALLWISE	A20	ALLWISE Identifier	–	–	–
9	GAIA	A20	<i>Gaia</i> Identifier	–	–	–
10	APASS	A30	APASS Identifier	–	–	–
11	KIC	I8	KIC Identifier	–	–	–
12	Objtype	A10	Object Type	–	–	–
13	Typesrc	A12	Source of the object	–	–	–
14	RA	D10.6	Right Ascension J2000	0	360	NN
15	Dec	D10.6	Declination J2000	-90	90	NN
16	Posflag	A12	Source of the position	–	–	–
17	pmRA	D10.3	Proper Motion in Right Ascension	-15000	15000	–
18	e_pmRA	D10.3	Uncertainty in Right Ascension	0	15000	–
19	pmDec	D10.3	Proper Motion in Declination	-15000	15000	–
20	e_pmDec	D10.3	Uncertainty in Declination	0	15000	–
21	PMFlag	A12	Source of the Proper Motion	–	–	–
22	plx	D10.3	Parallax	-100	1000	–

23	e_plx	D10.3	Error in the parallax	-100	1000	-
24	PARFlag	A12	Source of the parallax	-	-	-
25	GalLong	D10.6	Galactic Longitude	0	360	NN
26	GalLat	D10.6	Galactic Latitude	-90	90	NN
27	EcLong	D10.6	Ecliptic Longitude	0	360	NN
28	EcLat	D10.6	Ecliptic Latitude	-90	90	NN
29	Bmag	E6.3	Johnson <i>B</i>	-25	50	-
30	e_Bmag	E6.3	Uncertainty in Johnson <i>B</i>	0	50	-
31	Vmag	E6.3	Johnson <i>V</i>	-25	50	-
32	e_Vmag	E6.3	Uncertainty in Johnson <i>V</i>	0	50	-
33	umag	E6.3	Sloan <i>u</i>	-25	50	-
34	e_umag	E6.3	Uncertainty in Sloan <i>u</i>	0	50	-
35	gmag	E6.3	Sloan <i>g</i>	-25	50	-
36	e_gmag	E6.3	Uncertainty in Sloan <i>g</i>	0	50	-
37	rmag	E6.3	Sloan <i>r</i>	-25	50	-
38	e_rmag	E6.3	Uncertainty in Sloan <i>r</i>	0	50	-
39	imag	E6.3	Sloan <i>i</i>	-25	50	-
40	e_imag	E6.3	Uncertainty in Sloan <i>i</i>	0	50	-
41	zmag	E6.3	Sloan <i>z</i>	-25	50	-
42	e_zmag	E6.3	Uncertainty in Sloan <i>z</i>	0	50	-
43	Jmag	E6.3	2MASS <i>J</i>	-25	50	-
44	e_Jmag	E6.3	Uncertainty in 2MASS <i>J</i>	0	50	-
45	Hmag	E6.3	2MASS <i>H</i>	-25	50	-
46	e_Hmag	E6.3	Uncertainty in 2MASS <i>H</i>	0	50	-
47	Kmag	E6.3	2MASS <i>K_S</i>	-25	50	-
48	e_Kmag	E6.3	Uncertainty in 2MASS <i>K_S</i>	0	50	-
49	TWOMflag	A20	Quality Flags for 2MASS	-	-	-
50	prox	E6.3	2MASS Nearest Neighbor	0	500	-
51	W1Mag	E6.3	WISE W1	-25	50	-
52	e_W1Mag	E6.3	Uncertainty in WISE W1	0	50	-
53	W2Mag	E6.3	WISE W2	-25	50	-
54	e_W2Mag	E6.3	Uncertainty in WISE W2	0	50	-
55	W3Mag	E6.3	WISE W3	-25	50	-
56	e_W3Mag	E6.3	Uncertainty in WISE W3	0	50	-
57	W4mag	E6.3	WISE W4	-25	50	-
58	e_W4Mag	E6.3	Uncertainty in WISE W4	0	50	-
59	Gmag	E6.3	<i>Gaia</i> <i>G</i> Magnitude	-25	50	-
60	e_Gmag	E6.3	Uncertainty in <i>Gaia</i> <i>G</i>	0	50	-
61	Tmag	E6.3	TESS Magnitude	-4	50	NN
62	e_Tmag	E6.3	Uncertainty in TESS Magnitude	0	50	NN
63	TESSFlag	A5	TESS Magnitude Flag	-	-	-
64	SPFlag	A5	Stellar Properties Flag	-	-	-
65	Teff	E6.0	Effective Temperature	300	100000	-
66	e_Teff	E6.0	Uncertainty in Effective Temperature	0	100000	-
67	logg	E6.3	log of the Surface Gravity	-5	10	-
68	e_logg	E6.3	Uncertainty in Surface Gravity	0	2.5	-
69	M/H	E6.3	Metallicity	-7	2	-
70	e_M/H	E6.3	Uncertainty in the Metallicity	0	2.5	-
71	Rad	E8.3	Radius	0.001	10000	-

72	e.Rad	E8.3	Uncertainty in the Radius	0	10000	–
73	Mass	E8.3	Mass	0.01	500	–
74	e_Mass	E8.3	Uncertainty in the Mass	0	500	–
75	rho	E10.3	Stellar Density	0	10 ⁸	–
76	e_rho	E10.3	Uncertainty in the Stellar Density	0	10 ⁸	–
77	LumClass	A10	Luminosity Class	–	–	–
78	Lum	E10.3	Stellar Luminosity	0	10 ⁷	–
79	e_Lum	E10.3	Uncertainty in Luminosity	0	10 ⁷	–
80	d	E8.1	Distance	1	5 ⁹	–
81	e_d	E8.1	Uncertainty in the distance	0	5 ⁹	–
82	e(b-v)	E6.3	Color Excess	0	99 ⁹⁹⁹	–
83	e_e(b-v)	E6.3	Uncertainty in Color Excess	0	99 ⁹⁹⁹	–
84	numcont	I6	Number of Contamination Sources	0	999999	–
85	contratio	E8.6	Contamination Ratio	0	–	–
86	disposition	A10	disposition type	–	–	–
87	dup_id	I10	Points to the TIC ID	–	–	–
88	pri	EXX	Stellar Priority	0	1	–

Table 6:: Brief description of TIC contents and permitted ranges for all values.

C. Provenance Flags in the TIC

Column	Name	Flags	Description
13	Typesrc	hip	stellar source is hipparcos
...	...	cooldwarfs	stellar source is the cool dwarf list
...	...	2mass	stellar source is 2MASS
...	...	lepine	stellar source is SuperBlink
21	PMFlag	ucac4	proper motions from UCAC4
...	...	tgas	proper motions from Tycho2- <i>Gaia</i> Astrometric Solution
...	...	sblink	proper motions from SuperBlink
...	...	tycho2	proper motions from Tycho2
...	...	hip	proper motions from Hipparcos
24	PARFlag	tgas	parallax from Tycho2- <i>Gaia</i> Astrometric Solution
...	...	hip	parallax from Hipparcos
63	TESSFlag	tmvk	T calculated from 2MASS V , and K_S
...	...	joffset	T calculated from 2MASS J offset
...	...	joffset2	T calculated from 2MASS J offset
...	...	hoffset	T calculated from 2MASS H offset
...	...	koffset	T calculated from 2MASS H offset
...	...	voffset	T calculated from V offset
...	...	cdwarf	T calculated from cdwarf catalog (see Sec. E.1.1 & Muirhead et al. 2017)
...	...	from_apass_i	T calculated from cdwarf catalog (see Sec. E.1.1 & Muirhead et al. 2017)
...	...	from_sdss_i	T calculated from cdwarf catalog (see Sec. E.1.1 & Muirhead et al. 2017)
...	...	wmean_vk_jhk	T calculated from cdwarf catalog (see Sec. E.1.1 & Muirhead et al. 2017)
...	...	hipvmag	cool-dwarf?
...	...	lepine	cool-dwarf?
...	...	vjk	T calculated from Johnson V , 2MASS J & K_S
...	...	vjh	T calculated from Johnson V , 2MASS J & H

...	...	jh	T calculated from 2MASS J & H
...	...	jhk	T calculated from 2MASS J , H & K_S
...	...	bpjk	T calculated from Photographic B and 2MASS J & K_S
64	SPFlag	cdwarf	mass and radius provided by the Cool Dwarf list (see Sec. E.1.1 & Muirhead et al)
...	...	plx	characteristics computed from measured parallax
...	...	spect	characteristics computed using the spectroscopic Torres relations
...	...	allen	characteristics computed from T_{eff} using modified relations from Allens Astrophys
...	...	normal	same as allen, naming artifact to be removed in future releases

Table 7:: Brief description of flags in the TIC and CTL.

D. Internal Consistency in the TIC

As described above, the TIC is created by compiling numerous independent catalogs and using this information to calculate a variety of stellar parameters, in a variety of ways. This can lead to the final version of the TIC not being entirely self-consistent. Here we explain a variety of checks aimed at making the TIC as self-consistent as possible. This mainly includes ensuring various calculated parameters, which are dependent on other observed and calculated quantities, are calculated using the reported TIC values to avoid contradictory information for any given star. We provide a list of these internal consistency checks below:

1. **Various Columns:** V and other magnitudes

Dependencies: (1) T_{eff} and (2) radius, if the radius is from parallax and bolometric correction

Issues: The magnitudes might not be consistent with T_{eff} or other quantities if those quantities are taken from an override catalog (e.g., special targets list).

Implemented Fix: V from the Cool Dwarf list does not override the default TIC V for now.

2. **Column 65:** Effective temperature (T_{eff})

Dependencies: $E(B - V)$ and $[\text{Fe}/\text{H}]$ if from color

Issues: (1) T_{eff} might not agree with L_{bol} and radius, (2) T_{eff} will be different from dereddened phot-based value if from spectroscopy; (3) T_{eff} will be different from dereddened phot-based value and/or from spectroscopy if taken from cool dwarf list

Implemented Fix: T_{eff} is set to “NULL” if the cool dwarf list provides mass and radius but not T_{eff} .

3. **Column 67:** Surface Gravity ($\log g$)

Dependencies: Mass and Radius if not from spectroscopy

Issues: (1) $\log g$ will not in general agree with Mass and Radius if taken from spectroscopy.

Implemented Fix: We always calculate $\log g$ from mass (#73) and radius (#71) and ignore spectroscopic $\log g$.

4. **Column 71:** Radius

Dependencies: (1) Parallax, reddening, T_{eff} if from parallax; or (2) spectroscopic T_{eff} $\log g$ $[\text{Fe}/\text{H}]$ if from Torres et al. (2010) relations; or (3) T_{eff} if from Allen’s relations; or (4) cool dwarf list

Issues: No issues because radius is a primary derived quantity.

Implemented Fix: The radius is calculated from parallax when available.

5. **Column 73:** Mass

Dependencies: (1) spectroscopic T_{eff} $\log g$ [Fe/H] if from Torres et al. (2010) relations; (2) T_{eff} if from spline relations; or (3) cool dwarf list

Issues: No issues because mass is a primary derived quantity.

Implemented Fix: No need to fix.

6. **Column 75:** Density (ρ)

Dependencies: Mass and Radius if not from literature (e.g., transit based analysis)

Issues: ρ from literature (e.g., transit analysis) might not agree with calculated mass and radius

Implemented Fix: We calculate ρ from mass (#73) and radius (#71) if not from a transit analysis.

7. **Column 77:** Luminosity Class

Dependencies: Temperature and Radius (i.e., HR diagram position)

Issues: Luminosity class might be different from spectroscopic catalogs.

Implemented Fix: Currently the Luminosity Class is determined to be either a “dwarf” or “giant,” based on the RPM_J cut.

8. **Column 78:** Luminosity (L_{bol})

Dependencies: (1) Radius and T_{eff} if from Stefan Boltzmann, or (2) parallax, T_{eff} via BC, reddening.

Issues: Parallax based luminosity might not agree with T_{eff} and radius.

Implemented Fix: We always calculated L_{bol} from Stefan-Boltzmann. This will naturally include parallax based radii if radius is from parallax.

9. **Column 80:** Distance

Dependencies: (1) Parallax, or (2) invert Stefan-Boltzmann

Issues: Distance could be inconsistent with parallax.

Implemented Fix: We always calculated distance from parallax if available and less than 20% error. Otherwise use method 2 with V if available. Distance error set as “NULL” when derived by inverting Stefan-Boltzmann relation.

10. **Column 82:** $E(B - V)$

Dependencies: Color-color diagram reddening vector

Issues: Reddening will be inconsistent with that implied by Stefan-Boltzmann law if radius is obtained some way other than via parallax

Implemented Fix: This is a second-order effect and not fixed but is documented for completeness.

E. The use of special catalogs

The TIC uses a variety of uniform relations to calculate stellar parameters, such as T_{eff} and radius. Unfortunately, the majority of these relations are appropriate only for dwarf stars and may fail to accurately reproduce the appropriate physical parameters when applied to stars not considered a typical dwarf star (in the temperature range $3840 \text{ K} \lesssim T_{\text{eff}} \lesssim 10,000 \text{ K}$). The TESS Target Selection Working Group (TSWG) therefore has tasked the creation of special catalogs, listed below, to create an accurate list of stellar parameters for specific categories of targets, such as cool dwarfs. These catalogs also aim to include

high priority targets that may not be included in the CTL due to their unusual nature or poorly calculated default parameters for reasons described above.

The special target lists currently incorporated into TIC-5 are:

1. Cool Dwarfs: This list is meant to identify all dwarf stars with $T_{\text{eff}} \lesssim 3840$ K where the default TIC parameter calculations do a poor job of characterizing. The list contains a number of late K-dwarfs as well.
2. Bright Stars: This list is meant to identify all bright stars in the sky, $T < 6$.

The expected special target lists for future TIC versions are:

1. White Dwarfs
2. Known Planet Hosts
3. Hot Subdwarfs
4. Open Cluster Stars

E.1. High Level Descriptions of the Special Target Lists in TIC-5

E.1.1. The Cool Dwarf List

The Cool Dwarf list is a highly specialized list of stellar parameters for K-dwarf and M-dwarf stars ($T_{\text{eff}} < 4000$ K). We provide a basic overview of the catalog here but direct the reader to Muirhead et al. (2017, in prep) for a more detailed discussion.

The catalog itself is created using the SUPERBLINK catalog, cross matched with 2MASS and APASS. Dwarf stars are separated from giant stars using parallax measurements, when available, or the reduced proper motion criteria of Gaidos et al. (2014). T_{eff} is calculated from $r - J$, $r - z$, and $V - J$ color with an additional $J - H$ term to account for systematic effects of [Fe/H]. For stars with trigonometric parallax, masses and radii are calculated using the $M_{K_S} - R_*$ relation from Benedict et al. (2016) and Mann et al. (2015) respectively. For stars without trigonometric parallax, radius and mass are calculated using the $T_{\text{eff}} - R_*$ relation from Mann et al. (2015) and a newly developed relation between T_{eff} and M_* .

The Cool Dwarf list is treated like an override catalog and the values provided replace default calculated values for T , T_{eff} stellar radius and stellar mass. The catalog provides a value for V from the SUPERBLINK catalog but at this time these values do *not* override the V column in the TIC.

E.1.2. The Bright Star List

The bright star list is a catalog of all ($\sim 10,000$) bright ($T < 6$) sources in the TIC. These objects are included in the CTL regardless of whether the star passes the RPM_J cut. We compared the list of bright TIC objects to the Yale Bright Star catalog (hereafter, YBC) (Hoffleit & Jaschek 1991) and found $\sim 80\%$ of the YBC is in our Bright Star list. Nearly $\sim 90\%$ of objects in the YBC but missing from the bright star list include stars where $V > 6$ or V is not provided. In future versions of the TIC we plan to incorporate the YBC fully as the Bright Star special target list.

These stars have contamination calculated in the normal way. However, because many of these stars may not be typical dwarf stars (with $3850 < T_{\text{eff}} < 10000$), parameters such as radius and mass are not calculated unless the star already appears in the cool dwarf list or were previously identified as an RPM_J dwarf. Additionally, in TIC-5, these stars have a priority value of 1 as their priorities could not be effectively calculated using the schema described in § 3.3.

F. CTL Filtergraph Portal

Table 8 summarizes the contents of the enhanced CTL provided via the Filtergraph data visualization portal service at filtergraph.vanderbilt.edu/tess_ctl.

Descriptions of CTL Contents

Column name	Brief description
TICID	ID for the star in the TESS Input Catalog
Right_Ascension	RightAscension of the star, equinox J2000.0, epoch 2000.0 (degrees)
Declination	Declination of the star, equinox J2000.0, epoch 2000.0 (degrees)
Galactic_Long	Longitude in the Galactic coordinate frame (degrees)
Galactic_Lat	Latitude in the Galactic coordinate frame (degrees)
Ecliptic_Long	Longitude in the Ecliptic coordinate frame (degrees)
Ecliptic_Lat	Latitude in the Ecliptic coordinate frame (degrees)
Teff	Adopted ‘best’ value from (in order of preference): (1) Cool Dwarf list; (2) spectroscopic; (3) de-reddened photometric value; (4) non-dereddened photometric value. See Teff_Src column.
V_mag	Adopted <i>V</i> magnitude
J_mag	2MASS <i>J</i> magnitude
H_mag	2MASS <i>H</i> magnitude
K_mag	2MASS <i>K_S</i> magnitude
Hipparcos_Number	<i>Hipparcos</i> ID
Tycho2_ID	<i>Tycho-2</i> ID
2MASS_ID	2MASS ID
Priority_Non_Contam	Priority based on the <i>T</i> magnitude and stellar radius
Tess_mag	Calculated TESS magnitude
ContamRatio	Ratio of contaminating flux to flux from the star
Special_List	Flag to identify stars from the Cool Dwarf list (cdwarf), bright star list (bright) or both (cdwarf;bright)
Teff_Src	Source of the effective temperature (see Teff column)
Mass	Stellar mass derived from photometry (M_{\odot})
Radius	Stellar radius derived from photometry (R_{\odot})
Radius_src	Radius adopted from: torrallen (unified empirical spline relation); torplx (parallax); spectorr (spectroscopic); cdwarf (Cool Dwarf list)
Mass_src	Mass adopted from: torrallen (unified empirical spline relation); spectorr (spectroscopic); cdwarf (Cool Dwarf list)
Priority	Priority based on <i>T</i> , radius, and flux contamination with boosts and de-boosts
Priority_TIC_4	Priority based on <i>T</i> , radius, and flux contamination with boosts only from TIC-4

Table 8:: A basic description of all quantities found on the Filtergraph portal.

REFERENCES

- Alam, S., Albareti, F. D., Allende Prieto, C., et al. 2015, *ApJS*, 219, 12
- Altmann, M., Roeser, S., Demleitner, M., Bastian, U., & Schilbach, E. 2017, arXiv:1701.02629
- Ammons, S. M., Robinson, S. E., Strader, J., et al. 2006, *ApJ*, 638, 1004
- Bastien, F. A., Stassun, K. G., & Pepper, J. 2014, *ApJ*, 788, L9
- Bessell, M. S., & Brett, J. M. 1988, *PASP*, 100, 1134
- Benedict, G. F., Henry, T. J., Franz, O. G., et al. 2016, *AJ*, 152, 141
- Boeche, C., Siebert, A., Williams, M., et al. 2011, *AJ*, 142, 193
- Bovy, J., Rix, H.-W., Green, G. M., Schlafly, E. F., & Finkbeiner, D. P. 2016, *ApJ*, 818, 130
- Brewer, J. M., Fischer, D. A., Valenti, J. A., & Piskunov, N. 2016, *ApJS*, 225, 32
- Brown, T. M., Latham, D. W., Everett, M. E., & Esquerdo, G. A. 2011, *AJ*, 142, 112
- Burger, D., Stassun, K. G., Pepper, J., et al. 2013, *Astronomy and Computing*, 2, 40
- de Bruijne, J. H. J. 2012, *Ap&SS*, 341, 31
- Cardelli, J. A., Clayton, G. C., & Mathis, J. S. 1989, *ApJ*, 345, 245
- Casagrande, L., Flynn, C., & Bessell, M. 2008, *MNRAS*, 389, 585
- Casagrande, L., Ramírez, I., Meléndez, J., Bessell, M., & Asplund, M. 2010, *A&A*, 512, A54
- Ciardi, D. R., Beichman, C. A., Horch, E. P., & Howell, S. B. 2015, *ApJ*, 805, 16
- Cutri, R. M., Wright, E. L., Conrow, T., et al. 2013, Explanatory Supplement to the AllWISE Data Release Products, by R. M. Cutri et al. ,
- Collier Cameron, A., Wilson, D. M., West, R. G., et al. 2007, *MNRAS*, 380, 1230
- De Silva, G. M., Freeman, K. C., Bland-Hawthorn, J., et al. 2015, *MNRAS*, 449, 2604
- Duchêne, G., & Kraus, A. 2013, *ARA&A*, 51, 269
- Flower, P. J. 1996, *ApJ*, 469, 355
- Gaidos, E., Mann, A. W., Lépine, S., et al. 2014, *MNRAS*, 443, 2561
- Gilmore, G., Randich, S., Asplund, M., et al. 2012, *The Messenger*, 147, 25
- Girardi, L., Groenewegen, M. A. T., Hatziminaoglou, E., & da Costa, L. 2005, *A&A*, 436, 895
- Henden, A. A., Welch, D. L., Terrell, D., & Levine, S. E. 2009, American Astronomical Society Meeting Abstracts #214, 214, 407.02
- Hoffleit, D., & Jaschek, C. 1991, New Haven, Conn.: Yale University Observatory, c1991, 5th rev.ed., edited by Hoffleit, Dorrit; Jaschek, Carlos ,
- Holmberg, J., Nordström, B., & Andersen, J. 2009, *A&A*, 501, 941
- Høg, E., Fabricius, C., Makarov, V. V., et al. 2000, *A&A*, 355, L27

- Huang, Y., Liu, X.-W., Yuan, H.-B., et al. 2015, *MNRAS*, 454, 2863
- Huber, D., Bryson, S. T., Haas, M. R., et al. 2016, *ApJS*, 224, 2
- Husser, T.-O., Kamann, S., Dreizler, S., et al. 2016, *A&A*, 588, A148
- Kordopatis, G., Gilmore, G., Steinmetz, M., et al. 2013, *AJ*, 146, 134
- Kovács, G., Zucker, S., & Mazeh, T. 2002, *A&A*, 391, 369
- Kraus, A. L., Ireland, M. J., Huber, D., Mann, A. W., & Dupuy, T. J. 2016, *AJ*, 152, 8
- Lépine, S., & Gaidos, E. 2011, *AJ*, 142, 138
- Lindgren, L., Lammers, U., Bastian, U., et al. 2016, *A&A*, 595, A4
- Luo, A.-L., Zhao, Y.-H., Zhao, G., et al. 2015, *Research in Astronomy and Astrophysics*, 15, 1095
- Majewski, S. R., Schiavon, R. P., Frinchaboy, P. M., et al. 2015, arXiv:1509.05420
- Mann, A. W., Feiden, G. A., Gaidos, E., Boyajian, T., & von Braun, K. 2015, *ApJ*, 804, 64
- Newton, E. R., Irwin, J., Charbonneau, D., Berta-Thompson, Z. K., & Dittmann, J. A. 2016, *ApJ*, 821, L19
- Paegert, M., Stassun, K. G., De Lee, N., et al. 2015, *AJ*, 149, 186
- Pepper, J., Kuhn, R. B., Siverd, R., James, D., & Stassun, K. 2012, *PASP*, 124, 230
- Pepper, J., Pogge, R. W., DePoy, D. L., et al. 2007, *PASP*, 119, 923
- Perryman, M. A. C., Lindgren, L., Kovalevsky, J., et al. 1997, *A&A*, 323,
- Pojmanski, G. 1997, *Acta Astron.*, 47, 467
- Ricker, G. R., Winn, J. N., Vanderspek, R., et al. 2015, *Journal of Astronomical Telescopes, Instruments, and Systems*, 1, 014003
- Schlegel, D. J., Finkbeiner, D. P., & Davis, M. 1998, *ApJ*, 500, 525
- Schmidt, S., et al. 2016, *MNRAS*, in press
- Skrutskie, M. F., Cutri, R. M., Stiening, R., et al. 2006, *AJ*, 131, 1163
- Smith, A., & WASP Consortium 2014, *Contributions of Astronomical Observatory Skalnaté Pleso*, 43, 500
- Soubiran, C., Le Campion, J.-F., Brouillet, N., & Chemin, L. 2016, *A&A*, 591, A118
- Stassun, K. G., Collins, K. A., & Gaudi, B. S. 2017, *AJ*, 153, 136
- Sullivan, P. W., Winn, J. N., Berta-Thompson, Z. K., et al. 2015, *ApJ*, 809, 77
- Torres, G. 2010, *AJ*, 140, 1158
- Torres, G., Andersen, J., & Giménez, A. 2010, *A&A Rev.*, 18, 67
- Vanderburg, A., Plavchan, P., Johnson, J. A., et al. 2016, *MNRAS*, 459, 3565
- Warner, B. D. 2007, *Minor Planet Bulletin*, 34, 113
- York, D. G., Adelman, J., Anderson, J. E., Jr., et al. 2000, *AJ*, 120, 1579
- Zacharias, N., Finch, C. T., Girard, T. M., et al. 2013, *AJ*, 145, 44